

**UNIVERSITY OF CALIFORNIA**

Los Angeles

Up-Conversion of Terahertz Amplitude-Modulated CO<sub>2</sub> Laser Pulses Using  
Nonlinear Crystals

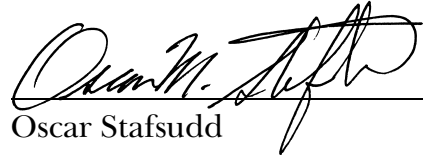
A thesis submitted in partial satisfaction of the requirements for  
the degree Master of Science in Electrical Engineering

by

Kari S. Sanders


2001

The thesis of Kari S. Sanders is approved.



---

Oscar Stafsudd



---

Warren Mori



---

Chandrashekhhar J. Joshi,  
Committee Chair

University of California, Los Angeles

2001

## TABLE OF CONTENTS

<b>1</b>	<b>Overview . . . . .</b>	<b>1</b>
<b>2</b>	<b>Frequency Conversion in Nonlinear Crystals . . . . .</b>	<b>5</b>
2.1	Second Harmonic Generation . . . . .	6
2.2	Sum Frequency Generation. . . . .	7
2.3	Phase Matching. . . . .	7
2.4	Acceptance Angle . . . . .	11
2.5	Efficiency . . . . .	12
2.6	Group Velocity Mismatch . . . . .	13
<b>3</b>	<b>SFG in AgGaS<sub>2</sub>. . . . .</b>	<b>14</b>
3.1	Crystal Selection for the THz Modulator . . . . .	14
3.1.1	Transparency . . . . .	15
3.1.2	Acceptance Angle . . . . .	15
3.1.3	Efficiency. . . . .	17
3.1.4	Group Velocity Mismatch . . . . .	18
3.1.5	Verification of Crystal Parameters for AgGaS <sub>2</sub> . . . . .	18
3.1.6	Summary. . . . .	20
3.2	Phase 1: SFG Using a fiber optic delay line . . . . .	21
3.2.1	Experimental Setup: Block Diagram. . . . .	22
3.2.2	Experimental Setup: Photos . . . . .	23
3.2.3	Equipment Selection . . . . .	24
3.2.4	Experimental Data . . . . .	30

3.3	Phase 2: SFG Using 100 ps CO <sub>2</sub> Pulses . . . . .	35
3.3.1	Experimental Setup . . . . .	35
3.3.2	Theoretical Efficiency and Output Power . . . . .	38
3.3.3	Experimental Data . . . . .	39
3.4	Summary . . . . .	42
<b>4</b>	<b>Up-Conversion in KDP . . . . .</b>	<b>43</b>
4.1	Theoretical Analysis . . . . .	43
4.2	Experimental Data . . . . .	44
<b>5</b>	<b>Detection of Modulation: Autocorrelation . . . . .</b>	<b>46</b>
5.1	Background . . . . .	46
5.2	Commercial Autocorrelator . . . . .	48
5.3	Custom Autocorrelator Design . . . . .	50
5.3.1	Experimental Setup . . . . .	51
5.3.2	Experimental Design. . . . .	52
5.3.3	Future Work . . . . .	52
<b>6</b>	<b>Conclusion . . . . .</b>	<b>53</b>

## LIST OF FIGURES AND TABLES

Figure 1-1: Concept Overview for PBWA Experiment. . . . .	1
Figure 1-2: Block Diagram of SFG . . . . .	2
Figure 1-3: CO <sub>2</sub> Pulse Train . . . . .	2
Figure 1-4: Chronological Overview . . . . .	4
Figure 2-1: Block Diagram of SHG . . . . .	6
Figure 2-2: Block Diagram of SFG . . . . .	7
Figure 2-3: Diagram of Phase Matching . . . . .	8
Figure 2-4: Sample Phase Matching Diagram for Collinear SHG . . . . .	9
Figure 2-5: Vector Addition for Noncollinear Phase Matching . . . . .	9
Figure 2-6: Samples of Phase Matching for Noncollinear SHG . . . . .	10
Figure 2-7: Sample Intensity Profile . . . . .	12
Table 3-1: Crystal Analysis, Acceptance Angle . . . . .	15
Figure 3-1: Theoretical Acceptance Angle for AgGaS <sub>2</sub> . . . . .	16
Figure 3-2: Phase Matching Curve for AgGaS <sub>2</sub> . . . . .	17
Table 3-2: Crystal Analysis, Group Velocity Mismatch. . . . .	18
Table 3-3: Values for d <sub>36</sub> in AgGaS <sub>2</sub> . . . . .	19
Table 3-4: Index of Refraction for 10.59 μm, AgGaS <sub>2</sub> . . . . .	20
Figure 3-3: Phase 1 Block Diagram . . . . .	22
Figure 3-4: Phase I Photo . . . . .	23
Figure 3-5: Phase I Interaction Point . . . . .	23
Figure 3-6: Beam Profile Data. . . . .	30
Figure 3-7: Image of Nd:YAG Pulse . . . . .	31

<b>Figure 3-8: Nd:YAG Pulse and CO<sub>2</sub> Pulse Train . . . . .</b>	<b>32</b>
<b>Figure 3-9: Nd:YAG and a Single CO<sub>2</sub> Pulse . . . . .</b>	<b>32</b>
<b>Figure 3-10: Spectrometer Image of AgGaS<sub>2</sub> Output . . . . .</b>	<b>34</b>
<b>Figure 3-11: One Line of Spectrometer Data, AgGaS<sub>2</sub> Output . . . . .</b>	<b>34</b>
<b>Figure 3-12: Phase 2: First Experimental Setup . . . . .</b>	<b>36</b>
<b>Figure 3-13: Crystal Orientation for Phase Matching Angle Scan . . . . .</b>	<b>37</b>
<b>Figure 3-14: Photo of Second Setup for Phase 2 . . . . .</b>	<b>37</b>
<b>Figure 3-15: AgGaS<sub>2</sub> Output Intensity Variation with 1 <math>\mu</math>m Input Energy .</b>	<b>39</b>
<b>Figure 3-16: Angular Dependence of SFG Output in AgGaS<sub>2</sub> . . . . .</b>	<b>40</b>
<b>Figure 3-17: Non-Collinear Phase Matching, Experimental Setup . . . .</b>	<b>41</b>
<b>Table 4-1: Theoretical Parameters for SHG, SFG in KDP . . . . .</b>	<b>44</b>
<b>Figure 4-1: Up-Conversion in KDP, Image . . . . .</b>	<b>45</b>
<b>Figure 4-2: Upconversion in KDP, Data . . . . .</b>	<b>45</b>
<b>Figure 5-1: Experimental Setup for Autocorrelation . . . . .</b>	<b>48</b>
<b>Figure 5-2: Collinear SHG in SSA with 1 <math>\mu</math>m Pulse, Path 1 . . . . .</b>	<b>49</b>
<b>Figure 5-3: Noncollinear SHG with two 1 <math>\mu</math>m Pulses . . . . .</b>	<b>49</b>
<b>Figure 5-4: Collinear SHG in SSA with 1 <math>\mu</math>m Pulse, Path 2 . . . . .</b>	<b>50</b>
<b>Figure 5-5: Block Diagram of Custom Autocorrelator . . . . .</b>	<b>51</b>
<b>Figure 5-6: Photo of Custom Autocorrelator . . . . .</b>	<b>51</b>

## ACRONYMS AND ABBREVIATIONS

AgGaS <sub>2</sub>	Silver Gallium Di-Sulphide, Silver Thiogallate
CCD	Charge-Coupled Device
CO <sub>2</sub>	Carbon Dioxide
CW	Continuous Wave
eV	Electron Volts, $1.6 \times 10^{-19}$ Joules per eV
FWHM	Full Width at Half Maximum
HeNe	Helium Neon. A HeNe laser produces red light (632 nm) and was used for optical alignment.
KDP	Potassium Dihydrogen Phosphate, KH <sub>2</sub> PO <sub>4</sub>
Nd:YAG	Neodymium, Yttrium, Arsenic, Garnet
mJ	Milli-Joules, $10^{-3}$ Joules
μm	Micrometer, $10^{-6}$ meters
nm	Nanometer, $10^{-9}$ meters
PBWA	Plasma Beat-Wave Acceleration
ps	Pico-seconds, $10^{-12}$ seconds
SFG	Sum Frequency Generation
SHG	Second Harmonic Generation
SSA	Single Shot Autocorrelator
THz	Terahertz, $10^{12}$ Hertz
UV	Ultra-Violet
VNIR	Very Near Infrared
ZnSe	Zinc Selenide

## **ACKNOWLEDGMENTS**

From UCLA, I thank Chan Joshi for his support and guidance. Thanks to Sergei Tochitsky many hours he has spent helping me in the lab and reviewing this paper. Thanks also to Catalin Filip for the time he spent on my project; to Ritesh Narang, Maria Guerrero, Ken Marsh, Chris Clayton, and Jerzy Hoffman for their help.

From Raytheon, I thank Bob Burley, Bob Knopf, and Angela Phillips, for their support throughout this process, as well as Todd Johnson and Robin Reeder for their advice re optical design.

Thanks to Kristin for the hours of consul and the benefit of her experiences. Thanks to Ali for all his encouragement and scholastic help. Thanks to Warren for patiently sitting through all my stories and for reviewing this paper. Thanks to Karen, Howard, Angela, Pete, Tim, Jeff, Jake, Laurie, Sacha, Todd, Alex, and Jarl for listening to my tales over and over and over again.

Thanks to our late cat, Gracie, for fuzz therapy and always being a joy to come home to.

Much thanks to my parents, my brother, Mike's parents, both our families, Eleanor, and Bill for their support and encouragement.

Most of all, thanks to my dear husband, Mike, for his enduring patience, for providing both encouragement and sympathy, for surviving my hectic schedule, and for always being there when I needed him.

## **ABSTRACT OF THE THESIS**

Up-Conversion of Terahertz Amplitude-Modulated CO<sub>2</sub>  
Laser Pulses Using Nonlinear Crystals

by

Kari S. Sanders

Master of Science in Electrical Engineering

University of California, Los Angeles, 2001

Professor Chandrashekhar Joshi, Chair

The purpose of this project was to demonstrate the up-conversion of THz modulation in a 10  $\mu\text{m}$  optical signal using a nonlinear crystal, AgGaS<sub>2</sub>. The motivation for this project is its possible application to the Plasma Beatwave Acceleration experiments. For these experiments, the electrons produced by the photocathode of an RF gun must be injected in phase with a relativistic plasma wave in order to experience acceleration. The plasma wave is produced using the beat frequency of two CO<sub>2</sub> laser wavelengths - 10.27 and 10.59  $\mu\text{m}$ . Since the photocathode requires UV light to efficiently produce electrons, the proposed method of synchronizing the laser pulses with the electrons was to up-convert the 1 THz modulation at 10  $\mu\text{m}$  three times using nonlinear crystals. The first crystal would produce Near-IR light, the second green, and the third UV. This project was a proof-of-principle experiment for the first stage of up-conversion.

The AgGaS<sub>2</sub> crystal was chosen because it is transparent to the wavelengths used and the group velocity mismatch between the incident wavelengths is sufficiently less than 1 ps to not distort the THz modulation as it passes through the medium. Sum Frequency Generation (SFG) was used to up-convert the laser pulses to 964 nm (SFG of 1.06 and 10.27  $\mu\text{m}$ ) and 967 nm (SFG of 1.06 and 10.59  $\mu\text{m}$ ). The nonlinear interaction was characterized using efficiency measurements and data describing the sum frequency output - in both its angular dependence and spectral distribution.

Two methods of detecting the 1 THz modulation were investigated. The first required the analysis of spectral data, where the modulation would be detected using the spectral side lobes it would create. This method was not successful. The second, autocorrelation, intended to detect the modulation by comparing the output of the crystal with a temporally shifted version of itself, through up-conversion the result in another nonlinear crystal. The first autocorrelator used could not detect the modulation, due to the low efficiency of SHG and the dispersive optical elements it used. Dispersive optics would spatially separate the two wavelengths, destroying the beat pattern. A second autocorrelator was constructed, but not tested. This device should measure 5.25 ps of the crystal output - enough to see the 1 ps modulation corresponding to the 1 THz beatwave.

This work successfully characterized the up-conversion of the 10  $\mu\text{m}$  pulses in the AgGaS<sub>2</sub> crystal, provided insight into the setup required to produce sufficient upconverted light, and made significant progress in setting the groundwork for future work.

## I OVERVIEW

The purpose of this project was to demonstrate the up-conversion of THz modulation in a 10  $\mu\text{m}$  optical signal. This is accomplished by mixing it with a 1  $\mu\text{m}$  pulse in a nonlinear crystal,  $\text{AgGaS}_2$ . One of the possible applications of this work is to provide picosecond synchronization and, eventually, phase-locking between the fast 10  $\mu\text{m}$  laser pulse and the electrons produced by the photocathode of the RF gun for the Plasma Beatwave Acceleration (PBWA) experiments.<sup>1,2</sup> The laser is used to produce a plasma and the electrons must be injected in phase with the relativistic plasma wave in order to be accelerated. Since the photocathode requires at least 100  $\mu\text{J}$  of UV light to efficiently produce electrons, the technological concept for the PBWA experiment is to up-convert the THz modulated signal three times - the first to produce 967 and 964 nm light, the second green light, and the third UV. This thesis project was a proof-of-principle experiment, intended to demonstrate the success of the first stage of up-conversion, in  $\text{AgGaS}_2$ .

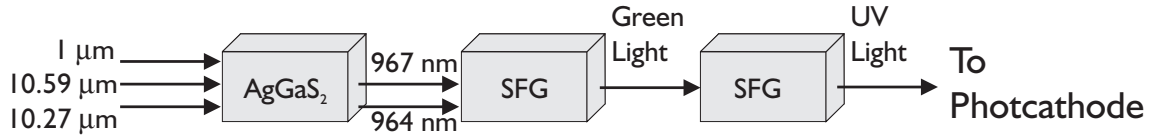


Figure 1-1: Concept Overview for PBWA Experiment

A nonlinear crystal was used for this experiment because the electrons within the solid material can react quickly enough (on the order of 10 fs) to transmit the 1 THz modulation. The experimental results hinge upon the up-conversion of THz modulation within the crystal, which occurs when the wavelength of an incident optical signal is changed. This process, when resulting in a shorter wavelength, is called up-conversion (Section 1.1). This project intended to demonstrate that the

original THz modulation was transmitted through the nonlinear crystal and was present at the new wavelength. Theoretical studies predicted that the 1 THz modulated wave should be transmitted by the  $\text{AgGaS}_2$  crystal with minimal distortion (Section 3.1.4), and the published literature demonstrated the detection of a similarly-generated 2.3 THz beat-wave signal using an autocorrelator.<sup>3</sup>

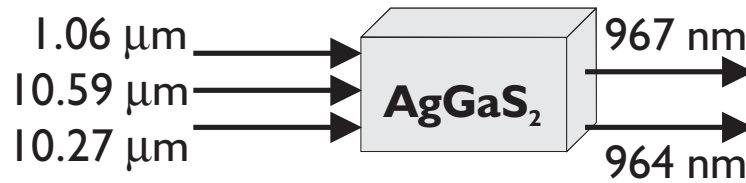


Figure 1-2: Block Diagram of SFG

Figure 1-2 shows the basic setup. The 1 THz amplitude-modulated signal is the beat frequency of two output lines of the  $\text{CO}_2$  laser. After amplification, the  $\text{CO}_2$  pulses are transported as a “pulse train”, as in the figure below.<sup>4</sup> (This is not the 1 THz modulation). The 1 THz amplitude modulation is the physical result of the

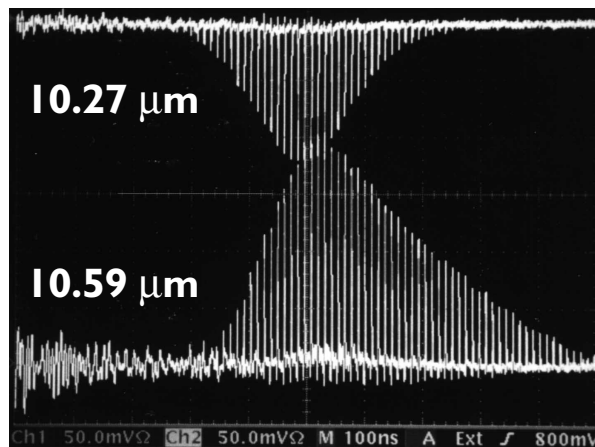


Figure 1-3:  $\text{CO}_2$  Pulse Train

beating between the two laser wavelengths. The two wavelengths - 10.27 and 10.59  $\mu\text{m}$  - are transported simultaneously in both time and space to preserve the THz beat frequency. An unmodulated 1  $\mu\text{m}$  signal is produced by a Nd:YAG laser. All three wavelengths are incident upon an  $\text{AgGaS}_2$  crystal, in which they were combined through a nonlinear optical process - Sum Frequency Generation (SFG, Section 2.2). The result was two shorter wavelengths, 964 nm (SFG of 1.06 and 10.27  $\mu\text{m}$ ) and 967 nm (SFG of 1.06 and 10.59  $\mu\text{m}$ ), with the 1 THz modulation impressed upon them.

Chronologically, there were three experimental phases for this project. During the first phase, up-conversion of the Nd:YAG and  $\text{CO}_2$  lasers was demonstrated. The planned use of spectral data to detect the modulation was unsuccessful, and there was insufficient power in the SFG output to try other means of detection. A second phase was constructed to better characterize the interaction and to provide sufficient power to try other methods of detection. The results of this phase included the successful characterization of two stages of up-conversion - the first in  $\text{AgGaS}_2$  and the second in a KDP crystal, resulting in green light; however, direct evidence of the THz modulation was lacking. Since the laboratory equipment could not directly measure THz frequencies, the modulation was to be detected using an autocorrelator (Section 5) - a device that optically compares two signals. For the third phase, a commercial autocorrelator was used, but the modulation could not be detected due to insufficient power and the presence of dispersive elements (Section 5), which spatially separated the two wavelengths, destroying the beat pattern. The final phase of the project was to use 6 ps pulses from a different Nd:YAG laser, instead of 100 ps, and a custom autocorrelator to

detect the modulation. This phase was not completed, due to time constraints, but an autocorrelator was designed and built for the purpose of detecting the modulation. The following figure pictorially shows the relationship between the three phases of the project.

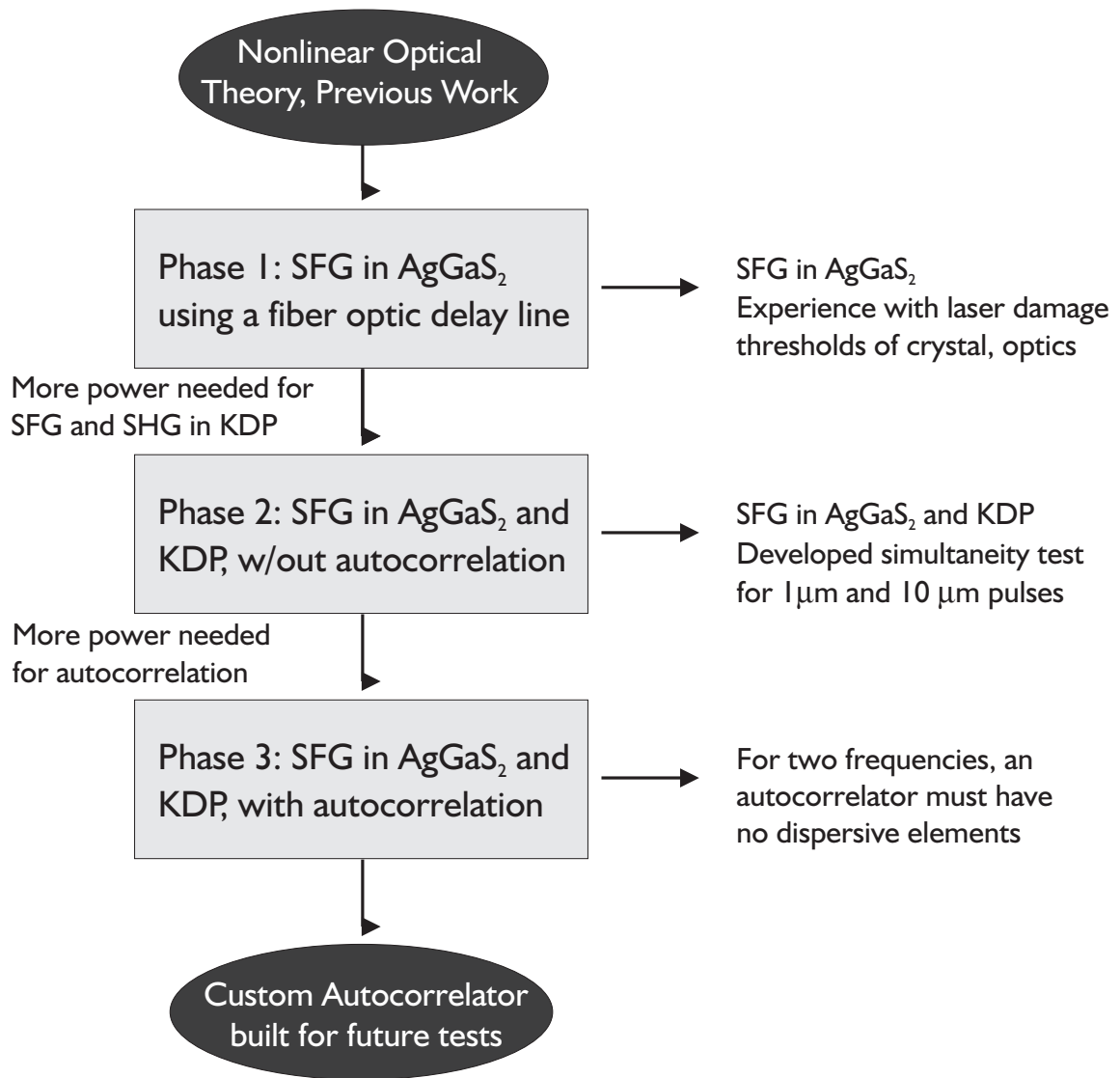


Figure 1-4: Chronological Overview

## 2 FREQUENCY CONVERSION IN NONLINEAR CRYSTALS

The theory of nonlinear optics describes the interaction of an electromagnetic wave, e.g., light, with a medium. In this case, the medium is a very specific kind of crystal - a negative uniaxial crystal.<sup>5</sup> (Section 3.1) The incident wave is described as an electric field,  $\vec{E}$ , with a polarization,  $\vec{P}$ . A uniaxial crystal has only one optical axis, defined as the plane along which the field may propagate without having its polarization changed. Ordinary waves,  $\vec{E}_o$ , are polarized perpendicular to the plane of the optical axis and experience an ordinary refractive index,  $n_o$ , as they propagate. Extraordinary waves,  $\vec{E}_e$ , are polarized in the plane of the optical axis and experience an extraordinary index of refraction,  $n_e$ . For a negative uniaxial crystal, such as AgGaS<sub>2</sub>,  $n_o > n_e$ .<sup>2</sup>

The field propagating through a nonlinear medium and its polarization are related by a tensor quantity, named the atomic susceptibility,  $\chi$ , as  $\vec{P} = \chi \vec{E}$ . The order of this tensor depends upon the order of the interaction within the medium. For example, both SFG (Sum Frequency Generation) and SHG (Second Harmonic Generation) are second order interactions, such that the susceptibility describing each is a tensor of rank 2 - a 3x3 matrix. The efficiency of a nonlinear interaction is proportional to the value of the susceptibility of the medium - i.e., the greater the susceptibility, the higher the efficiency.<sup>6</sup> (Section 2.5)

Two types of nonlinear interactions are employed by this project - SHG, which uses a single incident wavelength, and SFG, which uses two.

## 2.1 Second Harmonic Generation

In Second Harmonic Generation, a single incident wavelength is used to create an output wave with half the original wavelength.

$$\omega_{out} = \omega_{in} + \omega_{in} = 2\omega_{in} \quad (2.1)$$

If the crystal is transparent to the original wavelength, it passes through, as in the figure below. Note that the output wavelength, 532 nm in this case, would be spatially and temporally overlapped with the transmitted input wavelength for collinear phase matching and is shown to be dramatically separated in the figure only for illustrative purposes. (Note: Literally, some small separation of the beams would occur as they exit the crystal due to the walk-off angle, but this separation is not nearly as dramatic as that shown in the illustration.)

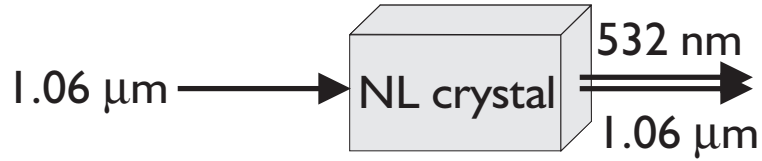


Figure 2-1: Block Diagram of SHG

The polarization of the resulting wave can be expressed as:

$$\vec{P}(\omega_2 = \omega_1 + \omega_1) = \chi^{(2)} : \vec{E}(\omega_1) \vec{E}(\omega_1) \quad (2.2)$$

This process was observed in the KDP crystal (section 4.2) and used to test the autocorrelator design, Section 5.3.

## 2.2 Sum Frequency Generation

In Sum Frequency Generation, two incident waves interact with the crystal to create an output wave corresponding to the sum of the incident frequencies:

$$\omega_{out} = \omega_{in1} + \omega_{in2} \quad (2.3)$$

As in Figure 2-1, the wavelengths are shown to be separated only for illustrative purposes.

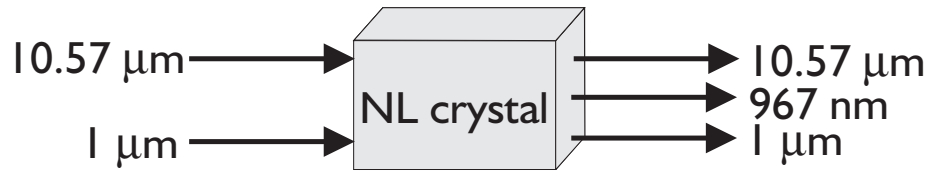


Figure 2-2: Block Diagram of SFG

The polarization of the resulting wave can be expressed as:

$$\vec{P}(\omega_3 = \omega_1 + \omega_2) = \chi^{(2)} : \vec{E}(\omega_1) \vec{E}(\omega_2) \quad (2.4)$$

## 2.3 Phase Matching

In order to maximize the efficiency of a nonlinear optical interaction, the incident wave(s) must be phase matched with the optical axis of the crystal. Phase matching refers to the synchronization of the phase velocities of the waves within the material.<sup>7</sup> The criterion for achieving this is generally expressed as the phase matching angle - the angle the incident wave must make with the optical axis of the crystal.

There are two types of phase matching: collinear, where the incident waves overlap in space, and noncollinear, where the waves intersect at a point within the crystal.

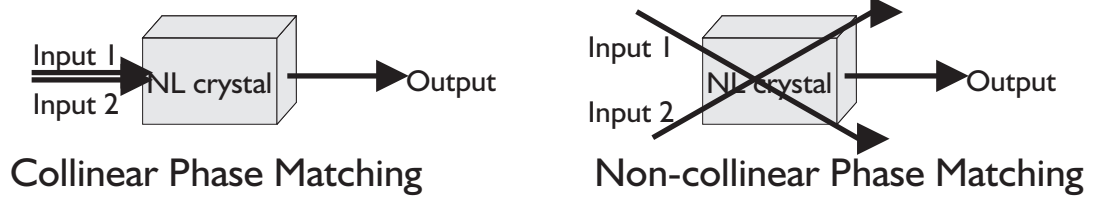


Figure 2-3: Diagram of Phase Matching

The phase matching angle is determined by the wavelengths involved in the interaction and their polarizations. This angle can be mapped by plotting the wave vectors,  $\vec{k}$ . For uniaxial birefringent nonlinear crystals,  $k = \frac{2\pi n_o}{\lambda}$  is constant with angle; whereas,  $n_e$  varies elliptically with the angle,  $\theta$ , from the optical axis,  $\vec{z}$ :<sup>2</sup>

$$k = \frac{2\pi n_e(\theta)}{\lambda} = \frac{2\pi n_o}{\lambda} \sqrt{\frac{1 + \tan^2 \theta}{1 + (n_o/n_e)^2 \tan^2 \theta}} \quad (2.5)$$

For collinear phase matching, the wave vectors add as scalars, as in Figure 2-4, and the phase matching angle is defined as the angle corresponding to when the curves for the resultant  $\vec{k}$  and the sum of the incident  $\vec{k}$ 's intersect.

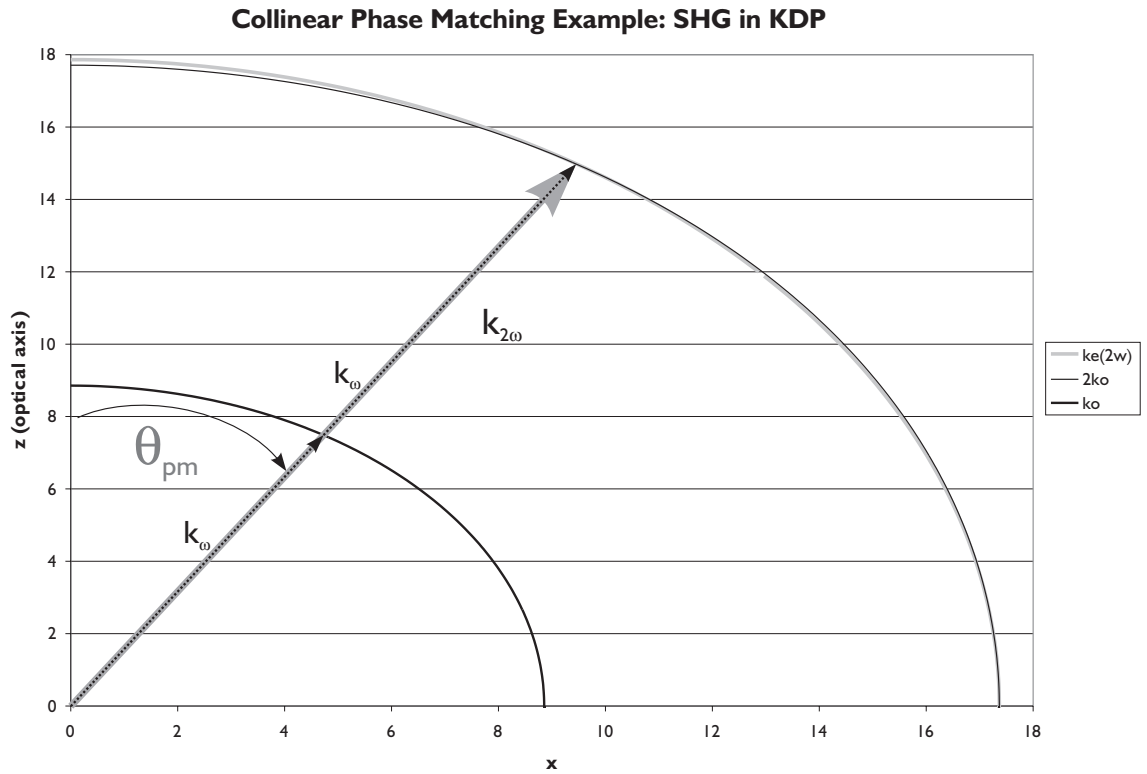


Figure 2-4: Sample Phase Matching Diagram for Collinear SHG

For noncollinear phase matching, the wave vectors add at an angle (the angle at which the incident wavelengths intersect), as in Figure 2-5.

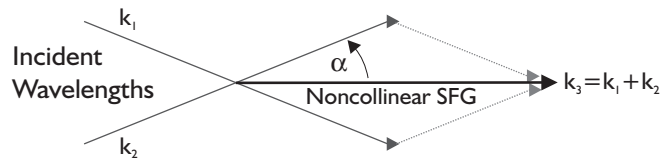


Figure 2-5: Vector Addition for Noncollinear Phase Matching

In vector addition, the phase matching condition,  $2k_{\omega 1} = k_{\omega 2}$  ( $k_1 + k_2 = k_3$  for SFG), is satisfied by:

$$2\left(\frac{2\pi n_{o1}}{\lambda_1}\right)\cos\alpha = \left(\frac{2\pi n_{o2}}{\lambda_2}\right)\sqrt{\frac{1 + \tan^2\theta}{1 + (n_{o2}/n_{e2})^2 \tan^2\theta}} \quad (2.6)$$

This condition can be fulfilled at a variety of angles, as shown in Figure 2-6.

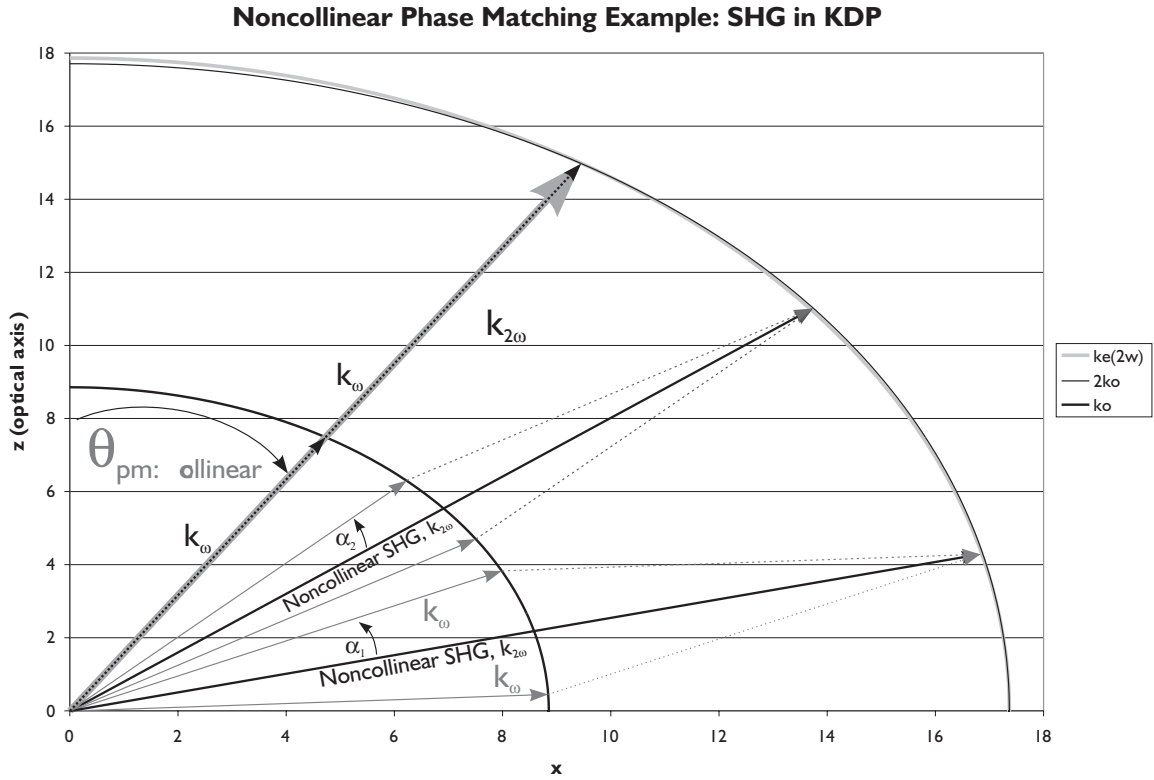


Figure 2-6: Samples of Phase Matching for Noncollinear SHG

There are two types of phase matching - “Type I” and “Type II”. Type I phase matching is used when two ordinary waves interact to produce an extraordinary wave. Type II phase matching is used when an ordinary and an extraordinary wave interact to produce a wave with extraordinary polarization. Since Type II

interactions have a larger group velocity mismatch, only Type I phase matching was used in this project. (Section 2.6) For a negative uniaxial crystal, the Type I phase matching angle can be calculated as:<sup>2</sup>

$$\text{Type I: } \tan^2 \theta_{pm}^{oe} = \frac{1-U}{W-1}, U = \frac{\left(\frac{n_{o1}}{\lambda_1} + \frac{n_{o2}}{\lambda_2}\right)^2}{\left(\frac{n_{o3}}{\lambda_3}\right)^2}, W = \frac{\left(\frac{n_{o1}}{\lambda_1} + \frac{n_{o2}}{\lambda_2}\right)^2}{\left(\frac{n_{e3}}{\lambda_3}\right)^2} \quad (2.7)$$

$$\text{Type I, noncollinear: } U = \frac{\left(\frac{n_{o1}}{\lambda_1}\right)^2 + \left(\frac{n_{o2}}{\lambda_2}\right)^2 + 2\left(\frac{n_{o1}}{\lambda_1}\right)\left(\frac{n_{o2}}{\lambda_2}\right)\cos\alpha}{\left(\frac{n_{o3}}{\lambda_3}\right)^2} \quad (2.8)$$

$$W = \frac{\left(\frac{n_{o1}}{\lambda_1}\right)^2 + \left(\frac{n_{o2}}{\lambda_2}\right)^2 + 2\left(\frac{n_{o1}}{\lambda_1}\right)\left(\frac{n_{o2}}{\lambda_2}\right)\cos\alpha}{\left(\frac{n_{e3}}{\lambda_3}\right)^2} \quad (2.9)$$

where  $\lambda_1$  and  $\lambda_2$  are the incident wavelength ( $\lambda_1=\lambda_2$  for SHG),  $\lambda_3$  is the output wavelength,  $n_o$  is the ordinary index of refraction and  $n_e$  is the extraordinary index of refraction, and  $\alpha$  is the angle between the incident waves.

## 2.4 Acceptance Angle

The acceptance angle is the range within which the incident beam may drift about the theoretical phase matching angle and produce little to no effect in the output wave. This angle,  $\Delta\theta$ , may be calculated using one of the following:<sup>2</sup>

$$\text{SHG, Type I: } \Delta\theta_{oe} = \frac{0.443\lambda_1 \left[1 + \left(\frac{n_{o2}}{n_{e2}}\right)^2 \tan^2 \theta\right]}{L \tan \theta \left|1 - \left(\frac{n_{o2}}{n_{e2}}\right)^2\right| n_2^e(\theta)} \quad (2.10)$$

$$\text{SFG, Type I: } \Delta\theta_{oe} = \frac{0.886\lambda_3 \left[1 + \left(\frac{n_{o3}}{n_{e3}}\right)^2 \tan^2 \theta\right]}{L \tan \theta \left|1 - \left(\frac{n_{o3}}{n_{e3}}\right)^2\right| n_3^e(\theta)} \quad (2.11)$$

where  $L$  is the length of the crystal,  $\theta$  is the incident angle,  $n_o$  is the ordinary index of refraction and  $n_e$  is the extraordinary index of refraction. For SHG,  $\lambda_1$  is the incident wave and  $\lambda_2$  is the output wave. For SFG,  $\lambda_1$  and  $\lambda_2$  are the incident waves and  $\lambda_3$  is the output wave.

The acceptance angle may be determined experimentally by plotting the variation of the output intensity with angle. The intensity varies as a sinc-squared function, as shown below, and the acceptance angle is estimated as the FWHM (Full Width at Half Maximum) of the zero<sup>th</sup> order lobe.<sup>4</sup>

$$I_{out} \propto \left[ \frac{\sin\left(\frac{\Delta k z}{2}\right)}{\frac{\Delta k z}{2}} \right]^2 \quad (2.12)$$

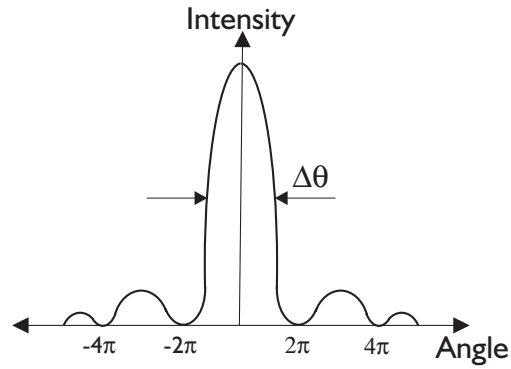


Figure 2-7: Sample Intensity Profile

## 2.5 Efficiency

The efficiency of the nonlinear interaction is the percent of the incident energy contained in the output wave and is calculated as:

$$\text{SHG: } \eta = \frac{P_{out}}{P_{in}} = \frac{2\pi^2 d_{eff}^2 L^2 P_{in}}{\epsilon_o c n_1^2 n_2^2 \lambda_2^2 A} \left( \frac{\sin\left(\frac{|\Delta k|L}{2}\right)}{\frac{|\Delta k|L}{2}} \right)^2 \quad (2.13)$$

$$\text{SFG: } \eta = \frac{P_{out}}{P_{in1}} = \frac{2^3 \pi^2 d_{eff}^2 L^2 P_2}{\epsilon_0 c n_1 n_2 n_3 \lambda_3^2 A} \left( \frac{\sin\left(\frac{|\Delta k|L}{2}\right)}{\frac{|\Delta k|L}{2}} \right)^2 \quad (2.14)$$

where  $d_{eff}$  is a parameter related to the atomic susceptibility (Section 2.0) of the medium,  $L$  is the crystal length,  $A$  is the area of interaction,  $c$  is the speed of light,  $\epsilon_0$  is the permittivity of free space, and  $\Delta k$  is approximated as  $\frac{0.886\pi}{L}$  for experimental purposes.<sup>2</sup>

## 2.6 Group Velocity Mismatch

Incident wavelengths will propagate at different speeds through a nonlinear crystal. If one considers two packets - groups - of photons with different wavelengths propagating simultaneously at one end of a crystal, then, by the time they reach the other end they will be separated by some amount of time. This temporal separation is called the group velocity mismatch. The time delay between pulses of two wavelengths for a specific crystal length,  $l$ , is calculated as below.<sup>8</sup>

$$t_g = \frac{length}{c} \left[ \lambda_1 \left( \frac{dn_1}{d\lambda_1} \right) - \lambda_2 \left( \frac{dn_2}{d\lambda_2} \right) \right], \text{ SHG} \quad (2.15)$$

$\frac{dn}{d\lambda}$  is calculated using the slope of the curve relating the index of refraction to the wavelength.<sup>9</sup> For SFG, the group velocity mismatch was estimated as  $\frac{\Delta n}{c}$ . The group velocity mismatch in the crystal is a crucial parameter for this experiment, as it must be small to maintain the 1 THz beat frequency.

### 3 SFG IN AgGaS<sub>2</sub>

#### 3.1 *Crystal Selection for the THz Modulator*

The AgGaS<sub>2</sub> crystal was purchased before I joined the project and was selected after a careful comparison of the standard crystals available. When comparing nonlinear crystals, one must consider attributes such as transparency, acceptance angle, efficiency for the proposed interaction, and group velocity mismatch. An analysis of the characteristics of AgGaS<sub>2</sub> is provided in this section.

Published literature indicates that this crystal was been widely used to up-convert mid-IR wavelengths. For example:

Bhar, Das, and Datta achieved Type II SFG using a CO<sub>2</sub> laser (10.6 mm), a Nd:YAG laser (1.06 mm), and a 6 mm thick AgGaS<sub>2</sub> crystal. The phase matching angle was 40.17°, the acceptance angle was 0.17°. <sup>10</sup>

Voronin et al achieved both Type I and Type II SFG of CW 10.6 μm and 1.06 μm lasers in a 5x5x3 mm AgGaS<sub>2</sub> crystal. The phase matching angle was 42°, and the interaction was approximately 40% efficient. <sup>11</sup>

Bhar et al used noncollinear phase matching of CO<sub>2</sub> and Nd:YAG pulses to achieve a Type II SFG interaction. The phase matching angle was 38.9°. A 5mm beam size and shorter pulses were used to increase the power that could be transmitted through the crystal without exceeding its damage threshold. <sup>12</sup>

### 3.1.1 Transparency

The material must be transparent to each wavelength that is used in the interaction. Transparency to the incident wavelengths allows them to interact with the entire length of the material, increasing the efficiency. Transparency to the resulting wavelength allows for the interaction to have an output. In this case, the material must be transparent to all wavelengths used in the interactions: 10.59  $\mu\text{m}$ , 10.27  $\mu\text{m}$ , 1.06  $\mu\text{m}$ , 0.967  $\mu\text{m}$ , and 0.964  $\mu\text{m}$ . The  $\text{AgGaS}_2$  crystal satisfies this requirement, with a transparency range of 0.47 - 13  $\mu\text{m}$ . A plot of the variation in the absorption coefficient of  $\text{AgGaS}_2$  with wavelength is available in Figure 4 of Reference 13.

### 3.1.2 Acceptance Angle

The acceptance angle,  $\Delta\theta$ , describes how much variation with respect to the phase matching angle the incident beams can have while maintaining the efficiency of the interaction. The acceptance angle was calculated using the equations shown in Section 2.4 and the Type I phase matching angle, coded in IDL. The results were multiplied by the refractive index of the output wave within the crystal to determine the external angle.

Phase Matching Angle (degrees)	Internal Acceptance Angle (degrees)	External Acceptance Angle (degrees)
37.6 (10.27 $\mu\text{m}$ )	0.309	0.745
37.3 (10.59 $\mu\text{m}$ )	0.311	0.749

Table 3-1: Crystal Analysis, Acceptance Angle

The figure below shows the relationship between the acceptance angle and the intensity profile for the proposed interaction. The phase matching angles are indicated at the peak of the  $\text{sinc}^2$  function (Figure 2-7) and the acceptance angle at the FWHM points. The overlap between these two curves indicates that the two SFG interactions -  $1.064\text{ }\mu\text{m}$  with  $10.27\text{ }\mu\text{m}$  and  $1.064\text{ }\mu\text{m}$  with  $10.59\text{ }\mu\text{m}$  - can be simultaneously phase matched using one crystal position. This concept is further supported by Figure 3-2, which demonstrates that the phase matching angle changes very little over the wavelength range of interest.

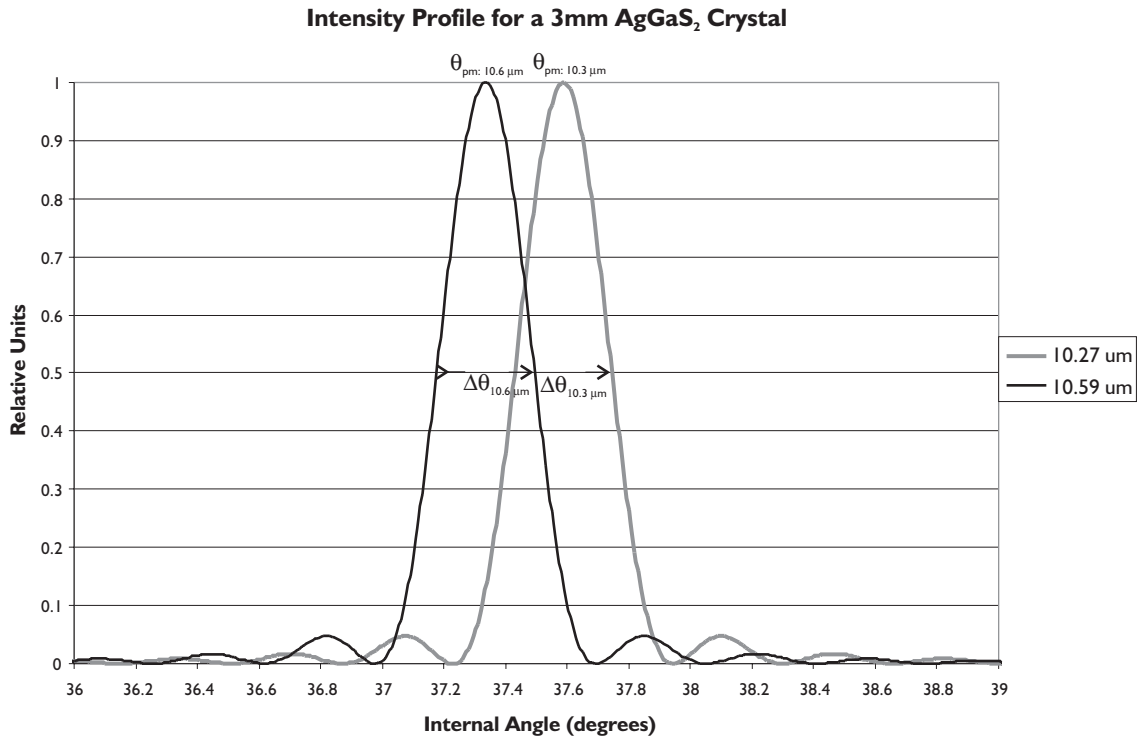


Figure 3-1: Theoretical Acceptance Angle for AgGaS<sub>2</sub>

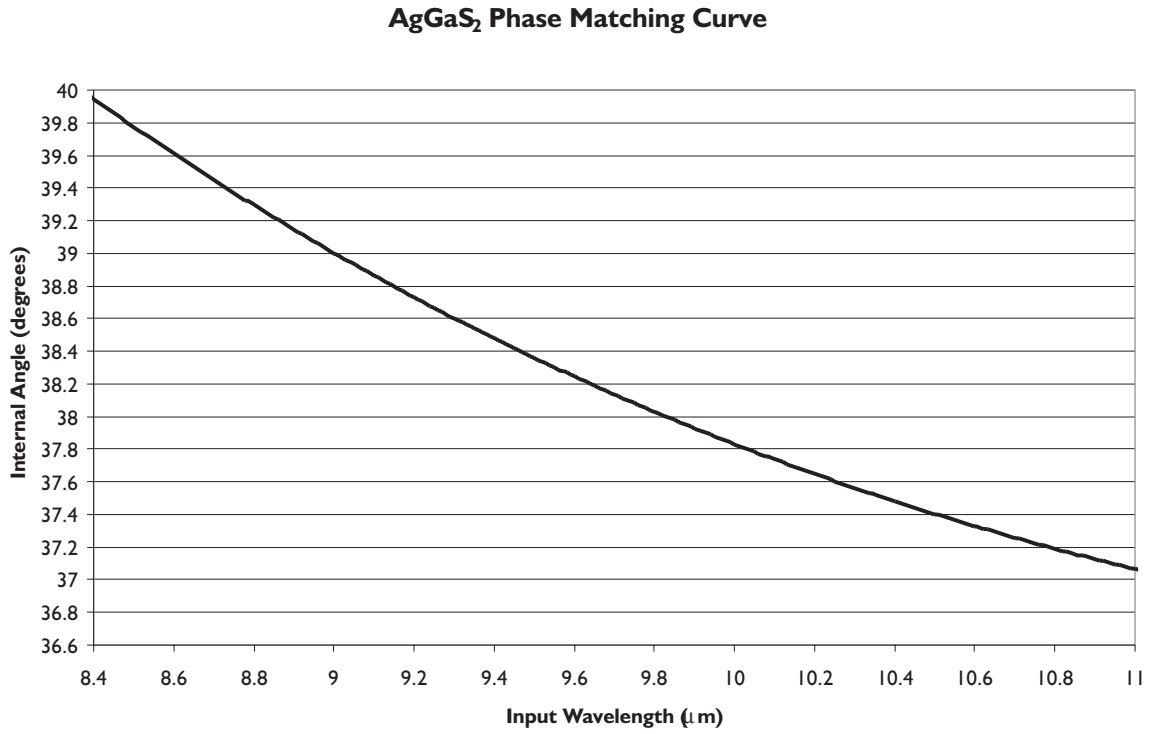


Figure 3-2: Phase Matching Curve for AgGaS<sub>2</sub>

### 3.1.3 Efficiency

A high efficiency is preferable, because less of the incident light is wasted. The efficiency was calculated for Phase 1 using the equation in Section 2.5, coded in IDL. For these calculations, the 1 μm power was assumed to be at the damage threshold of the crystal, 500 MW/cm<sup>2</sup>, focused to a spot with a radius of 50 μm. For 10.27 μm, the efficiency was calculated as 0.145%, and 0.142% for 10.59 μm.

### 3.1.4 Group Velocity Mismatch

For this experiment, the group velocity mismatch in the crystal must be small enough to preserve the 1 ps pulses in the modulated signal. For all of the interacting wavelengths, the AgGaS<sub>2</sub> crystal has a sufficiently small group velocity mismatch to preserve 1 ps pulses.

<b>Wavelengths (<math>\mu\text{m}</math>)</b>	<b>Group Velocity Mismatch (ps/cm)</b>
10.27 and 1.06	2.2
10.59 and 1.06	2.9

Table 3-2: Crystal Analysis, Group Velocity Mismatch

### 3.1.5 Verification of Crystal Parameters for AgGaS<sub>2</sub>

Many of the parameters used in the calculations for Sections 3.1-3.4 were derived from the Handbook of Nonlinear Optical Crystals.<sup>5</sup> A literature search was performed to verify the values used in the handbook, such as the effective nonlinear coefficient,  $d_{\text{eff}}$ , and the indices of refraction.

The value of the effective nonlinear coefficient is wavelength dependent and proportional to the efficiency of a nonlinear interaction. For AgGaS<sub>2</sub>,  $d_{eff} = d_{36} \sin(\theta) \sin(2\phi)$ ,<sup>2</sup> and the value of  $d_{36}$  has been reported in several publications.<sup>13,14,15</sup>

$d_{36}$ (pm/Volt)	Wavelength ( $\mu\text{m}$ )	Reference
$11.1 \pm 1.7$	10.6	5
$12.5 \pm 2.5$	10.6	5
$18 \pm 30\%$	10.6	13
14.5	1.06	14
11.2	10.6	15

Table 3-3: Values for  $d_{36}$  in AgGaS<sub>2</sub>

The index of refraction was calculated using the Sellmeier equation in the handbook.

$$n^2(\lambda) = A + \frac{B\lambda^2}{\lambda^2 - C} + \frac{D\lambda^2}{\lambda^2 - F} \quad (3.1)$$

The value for the index of refraction was also calculated using the Sellmeier

$n_e$ , 10.59 $\mu\text{m}$	$n_o$ , 10.59 $\mu\text{m}$	Reference
2.29293	2.34695	5
2.2934	2.3472	16
2.29847	2.35232	17
2.29261	2.34678	18
2.29280	2.34681	19
2.292	2.352	20
2.29293	2.34700	14

Table 3-4: Index of Refraction for 10.59  $\mu\text{m}$ ,  $\text{AgGaS}_2$

coefficients from several publications, as in Table 3-6.<sup>16,17,18,19,20</sup>

### 3.1.6 Summary

$\text{AgGaS}_2$  was chosen for this project because it is transparent to the wavelengths of interest, has a low group velocity mismatch, and has a sufficiently wide acceptance angle to allow phase matching of SFG with 10.27 and 10.59  $\mu\text{m}$  simultaneously.

### **3.2    *Phase I: SFG Using a fiber optic delay line***

The first phase of the experiment was designed to work independently of the PBWA experiments. The results of this phase were encouraging and provided much experience working with the crystal, but, due to a lack of incident power and success with spectral analysis of the output, the construction of a new setup was necessary (Section 3.3).

### 3.2.1 Experimental Setup: Block Diagram

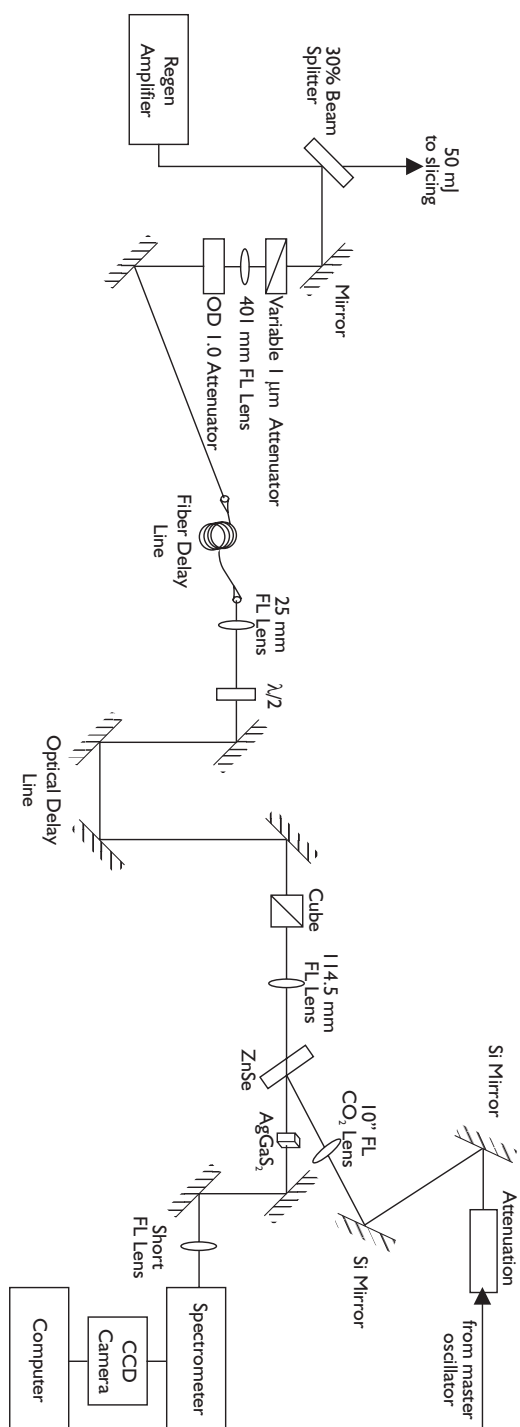


Figure 3-3: Phase 1 Block Diagram

### 3.2.2 Experimental Setup: Photos

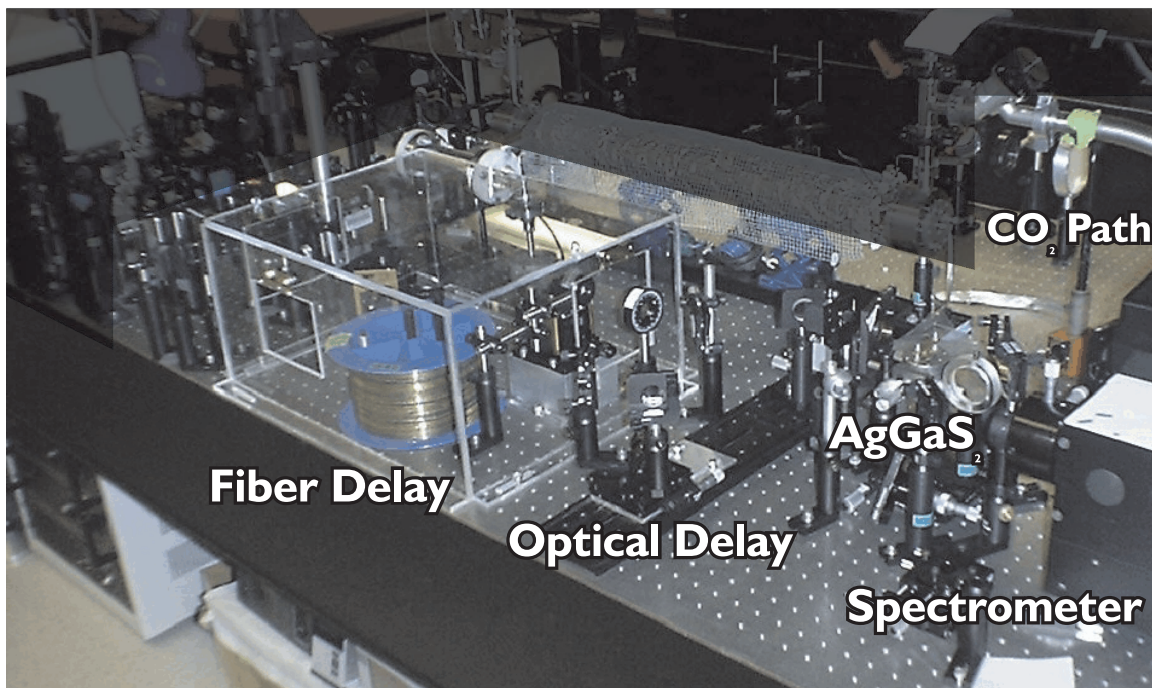


Figure 3-4: Phase I Photo

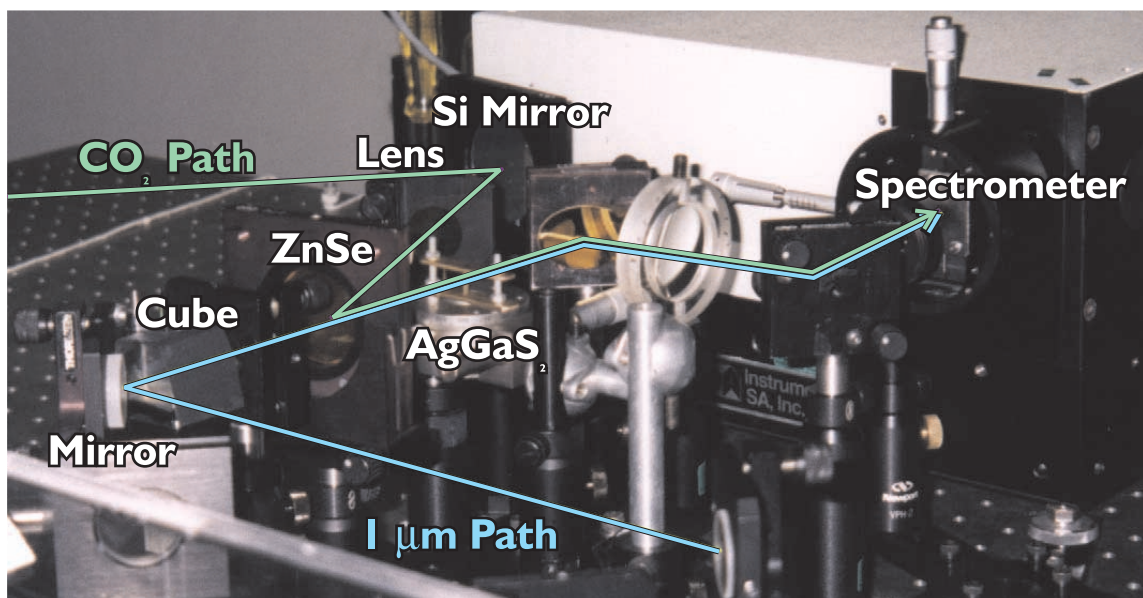


Figure 3-5: Phase I Interaction Point

### 3.2.3 Equipment Selection

Each component of the system was analyzed prior to construction. This section provides an overview of the theoretical work used to perform trade analyses and select equipment.

#### 3.2.3.1 *CO<sub>2</sub> Optical Path*

The manufacturer specified the damage threshold for the crystal at CO<sub>2</sub> wavelengths as 20 MW/cm<sup>2</sup> for 100 ns pulses. The final setup did not use a lens to focus the CO<sub>2</sub> pulses upon the AgGaS<sub>2</sub> crystal, because the shot-to-shot drifts in pulse power were sufficient to threaten damage to the crystal.

#### 3.2.3.2 *Nd:YAG Optical Path*

The main components of the 1  $\mu$ m optical path were the lenses used for coupling the pulses into and out of the optical fiber, the optical delay line (used for fine adjustments to the delay for purposes of synchronization) and the lens that focuses the pulses on the crystal. Other components were used for controlling the laser power (attenuation) and adjusting the polarization (half waveplate and cube).

##### 3.2.3.2.1 *Optical Fiber Delay Line*

An optical fiber was used to provide most of the delay required to synchronize the Nd:YAG and CO<sub>2</sub> pulses, because a long length of it could easily be placed on the table (in a spool). The design of the optical delay line included consideration for the surface damage threshold of the glass and methods for coupling the pulses to the fiber.

The limiting factor for this phase was the surface damage threshold of the optical fiber. The surface damage threshold was estimated as 10 GW/cm<sup>2</sup> from the surface damage threshold of silica,<sup>21,22,23,24,25</sup> which is approximately 30% less than that of

the bulk material.<sup>26,27</sup> In order to maintain a high damage threshold, the tip of the fiber must be carefully polished and kept dust-free.<sup>12,28</sup> The polishing was performed professionally by Fujiko Guth of Innova Quartz. A plexiglass case was constructed to minimize dust collection.

The fiber delay was designed to deliver 20  $\mu\text{J}$  of 1  $\mu\text{m}$  light to the crystal. A 200  $\mu\text{m}$  core, graded index silica/silica multimode fiber (WF-L22-201 from Wave Optics) was used. The length of the fiber was 86 m - to compensate for the 309 ns time delay between the  $\text{CO}_2$  and Nd:YAG pulses and the 123 ns delay from transporting the beam to the setup, assuming a refractive index of 1.5.

#### 3.2.3.2.1.1 Scattering and Self-Phase Modulation

Consideration was given to the possibility that the optical fiber could change the pulses, through mechanisms such as self-phase modulation, or lose energy to scattering mechanisms. Theoretical studies demonstrated that the scattering losses should not affect the fiber transmission, and analysis of the fiber's output with the spectrometer did not detect spectral broadening.

##### 3.2.3.2.1.1.1 Raman and Brillouin Scattering

Scattering within the fiber is likely to occur with high incident intensities. Both Raman and Brillouin scattering cause losses by propagating some of the incident light backward. The threshold intensities for these processes are approximately 15  $\text{MW}/\text{cm}^2$  for Raman scattering and 80  $\text{kW}/\text{cm}^2$  for Brillouin scattering<sup>29</sup>, both of which are below the typical operating intensity of 3.9  $\text{GW}/\text{cm}^2$  (when the 1  $\mu\text{m}$  pulses are focused upon the fiber). Thus, losses from scattering would be expected.

### 3.2.3.2.1.1.2 Self-Phase Modulation

If the intensity incident upon the fiber exceeded the threshold for self-phase modulation, one would expect to see frequency effects, such as chirping, in the pulses exiting the fiber. The threshold intensity for self-phase modulation may be calculated as follows:<sup>30</sup>

$$I_0 = \frac{\lambda}{2\pi n_2 L} \quad (3.2)$$

where  $n_2$ , the nonlinear index of refraction for silica, is approximately  $2.4 \times 10^{-16} \text{ cm}^2/\text{W}$ .<sup>31,32</sup>

For an 86-meter fiber, the intensity threshold for self-phase modulation is  $8.2 \text{ MW/cm}^2$ . Typically,  $30 \text{ } \mu\text{J}$  was incident upon the fiber in a spot with a  $50 \text{ } \mu\text{m}$  radius. This corresponds to an intensity of  $3.9 \text{ GW/cm}^2$ , which far exceeds the self-phase modulation threshold. The resolution of the spectrometer was insufficient to measure the chirp this produced, and no data was available after the scan angle for the crystal was corrected (Section 3.3.1.1) to determine the effects of this chirp upon the SFG output.

### 3.2.3.2.1.2 Coupling Lens Selection

Two lenses were needed for coupling the Nd:YAG pulses to the optical fiber. Traditionally, this coupling is performed using short focal length lenses or microscope objectives.<sup>33</sup> These methods are employed in order to properly launch the light into the fiber, which consists of two layers of glass, such as doped silica. The critical parameters are the angle at which the light enters the fiber and its position on the tip of the fiber, and the efficiency of the coupling is very sensitive to both. A significant decrease in the coupling efficiency may occur with a 10 to 20  $\mu\text{m}$  change in the position of the beam on the fiber or a 2 to 5 degree change in the incident angle.<sup>34</sup> Short focal length lenses are therefore typically used to provide better control over both the position and the angle of the input light.

The problem with using short focal length lenses for this project is that, due to the small spot size produced, the intensity delivered to the fiber would far exceed its damage threshold. To determine the spot size produced on the fiber by the short focal length lenses, the non-Gaussian beam profile of the Nd:YAG laser must be accounted for. The deviation of the beam from a Gaussian profile is described by  $M^2$ , equal to 2.5 for this laser.<sup>35</sup> The spot size,  $w_o$ , was calculated as shown below.<sup>36</sup>

$$w_o = \frac{2\lambda M^2 f}{\pi D} = 3.4\mu\text{m} \quad (3.3)$$

$$f = 25\text{mm}, D = 1.25\text{cm}, \lambda = 1.064\mu\text{m}, M^2 = 2.5 \quad (3.4)$$

A standard lens with a focal length of 401 mm was chosen to focus the pulses on the tip of the fiber - producing a spot size of approximately 135  $\mu\text{m}$ .

The light exiting the fiber quickly diffracts, necessitating a short focal-length lens to collect it. The theoretical angle of diffraction may be calculated using the fiber's numerical aperture. The numerical aperture for the fiber is defined using the difference in refractive index between the core and the cladding,

$$NA = n_1 \sqrt{2 \left( \frac{n_1^2 - n_2^2}{2n_1^2} \right)} \quad (3.5)$$

where  $n_1$  is the refractive index of the core and  $n_2$  is the refractive index of the cladding that surrounds the core.<sup>37</sup> The numerical aperture can also be expressed as the sine of the acceptance angle of the fiber.<sup>38</sup> For WF-L22-201 graded index multimode fiber from Wave Optics, Inc., the numerical aperture is 0.22.<sup>39</sup> The exit angle of the fiber is  $\theta = \sin^{-1}(0.22) = 12.7^\circ$ . Using a HeNe laser, a ruler, and a white screen, the diffraction angle was measured as  $11.8^\circ \pm 0.3^\circ$ . A standard lens with a one-inch focal length was chosen to collect the light exiting the fiber.

### 3.2.3.2.1.3 Alternate Delay Design

The optical fiber was originally chosen as a less expensive and time-consuming method of achieving the necessary delay for the Nd:YAG pulses. The drawback to this method was that it severely limited the 1  $\mu\text{m}$  power incident upon the crystal. Other options, which would have allowed a much greater input power, was to create an optical delay using mirrors. One such design uses two curved mirrors that can be configured on the same axis to create a lissajous pattern<sup>40</sup> or off-axis for a tighter pattern requiring less space.<sup>41</sup> Another design uses one flat mirror and curved mirror.<sup>42</sup> In either case, the light enters and exits the cavity through a hole in one of the mirrors, and the number of passes within the cavity is set by the angle at which the light enters, the curvature of the mirrors, and their spacing.

#### 3.2.3.2.2 *Focusing Lens*

The lens used to focus the Nd:YAG pulses on the crystal was chosen to deliver an intensity of  $500 \text{ MW/cm}^2$  to the crystal - approximately half the damage threshold quoted by the manufacturer for 100 ps pulses.

#### 3.2.3.2.3 *Optical Delay Line*

The purpose of the optical delay line was to provide a fine adjustment of the delay between the Nd:YAG and  $\text{CO}_2$  pulses. The line consisted of four mirrors, two of which were on a translational stage, allowing the length of the delay path to change ( $1 \text{ mm} = 3.33 \text{ ps}$ ). The mirrors were gold-coated, reflecting both  $1 \mu\text{m}$  and visible light for alignment purposes.

#### 3.2.3.3 *Beam Combiner*

For collinear phase matching, the Nd:YAG and  $\text{CO}_2$  pulses must overlap spatially as well as temporally. To achieve this, ZnSe was used as a beam combiner. One side of the ZnSe was coated to reflect  $10 \mu\text{m}$  light with 98.5% efficiency and the material transmitted  $1 \mu\text{m}$  light with  $75\% \pm 7\%$  efficiency (as measured experimentally).

#### 3.2.3.4 *Detection Systems*

Three types of detection were used in this phase: a photodetector, an energy meter, and a CCD carefully aligned at the output of a spectrometer. The photodetector provided relative power measurements for purposes of determining alignment and efficiency. The energy meter provided absolute energy measurements, used to verify that the laser power was below the crystal's surface damage threshold. The spectrometer provided frequency analysis of the crystal output. This spectral information was mapped spatially and collected using a CCD.

### 3.2.4 Experimental Data

#### 3.2.4.1 Beam Profile Measurement

To ensure that the Nd:YAG pulses were properly collected after exiting the optical fiber, the beam profile was measured using a micrometer and photodiode. The photodiode was stepped through the beam and a number of data points were collected at each position.

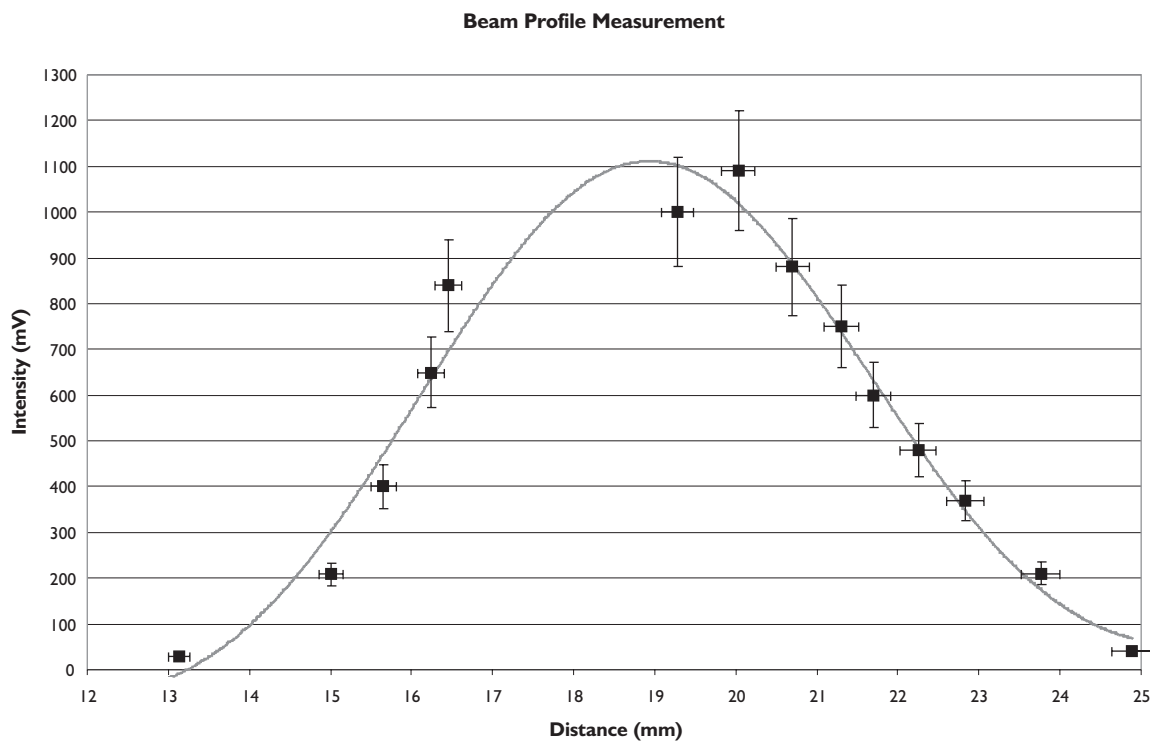


Figure 3-6: Beam Profile Data

The profile was also examined using a Cohu camera. The figure below shows the image of the beam, with its horizontal (left) and vertical (right) profiles below.

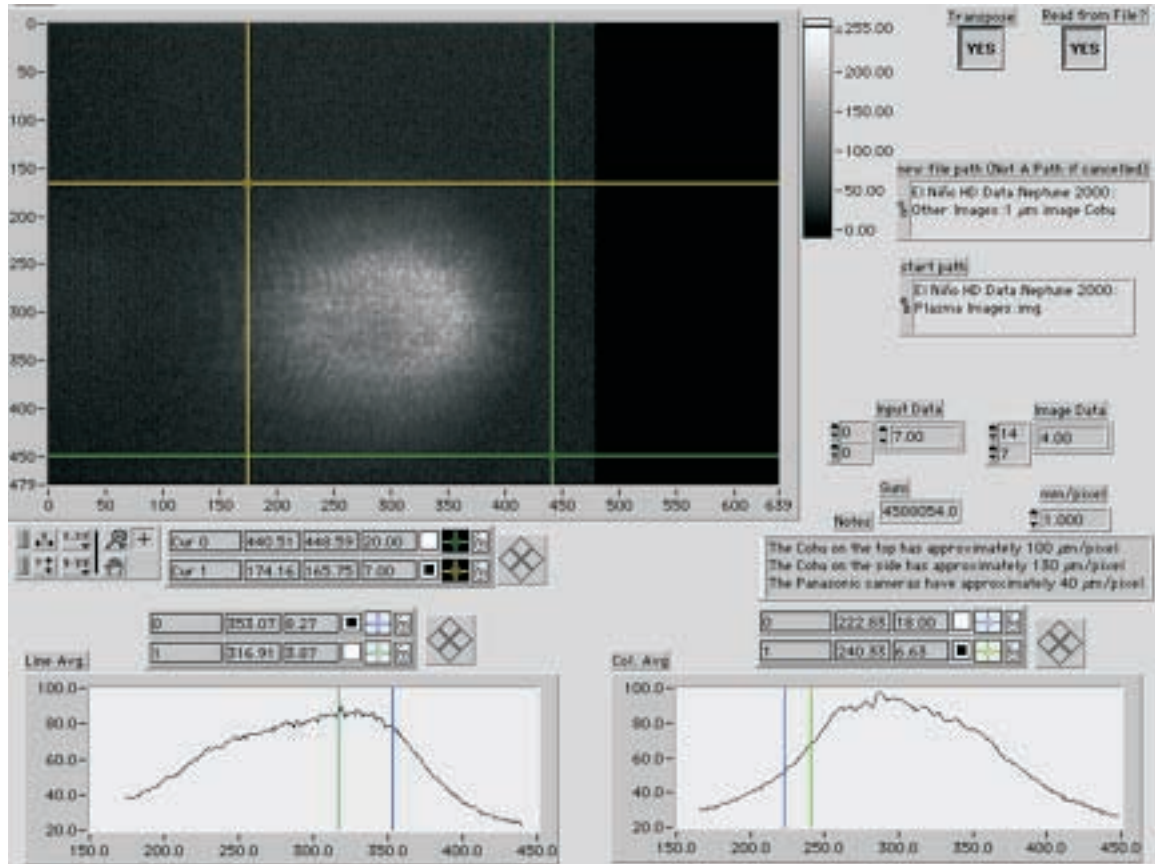


Figure 3-7: Image of Nd:YAG Pulse

### 3.2.4.2 Pulse Synchronization

The Nd:YAG (bottom trace) and CO<sub>2</sub> pulses (top trace) were temporally aligned, as shown in the following figures.

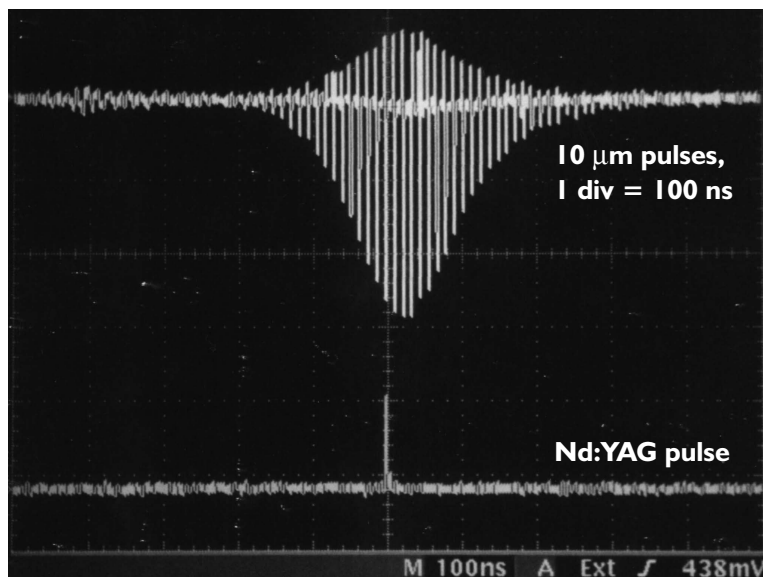


Figure 3-8: Nd:YAG Pulse and CO<sub>2</sub> Pulse Train

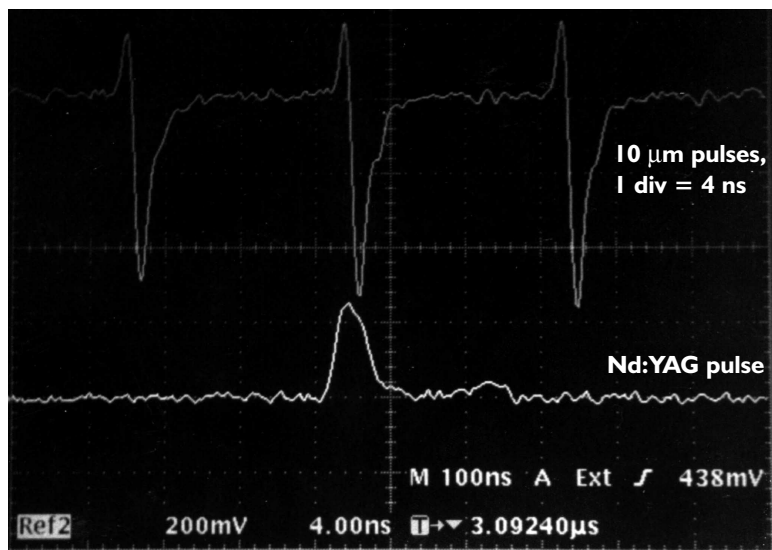


Figure 3-9: Nd:YAG and a Single CO<sub>2</sub> Pulse

### 3.2.4.3 SFG in AgGaS<sub>2</sub>

#### 3.2.4.3.1 Efficiency of Coupling to Optical Fiber

The maximum efficiency of the coupling to the optical fiber was measured as  $19\% \pm 6\%$  using a photodiode. The average coupling efficiency for measurements was 15%, and the efficiency was remeasured for each set of data to verify that the alignment had not drifted.

#### 3.2.4.3.2 Efficiency of SFG

The combined efficiency of the SFG interactions was estimated as  $0.4\% \pm 0.03\%$ , using a photodiode and calculating  $\eta \approx \frac{P_{967nm} + P_{964nm}}{P_{1\mu m}}$ . By this estimation, each interaction ( $10.59 \mu\text{m} + 1.06 \mu\text{m} \rightarrow 966 \text{ nm}$  or  $10.27 \mu\text{m} + 1.06 \mu\text{m} \rightarrow 964 \text{ nm}$ ) would have an efficiency slightly less than 0.2%, which is in agreement with the theoretical calculations in Section 3.1.3.

#### 3.2.4.3.3 Spectral Data

The output of the AgGaS<sub>2</sub> crystal was also viewed with a CCD at the output of the spectrometer, for purposes of determining the frequency of the outputs and for detecting the modulation (Section 3.2.4.4). Figure 3-10 shows the spectrometer output, and Figure 3-11 is a plot of one line of spectrometer data. A grating with 1200 grooves/mm was used with a 64  $\mu\text{m}$  slit.

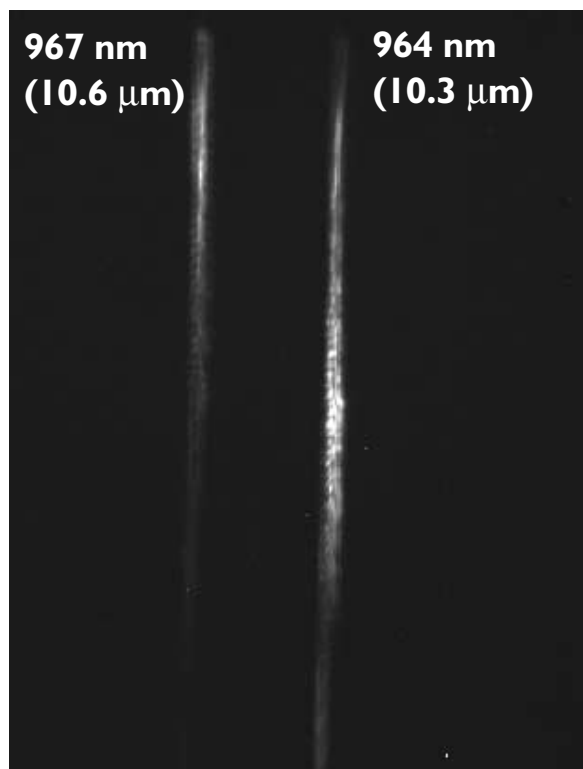


Figure 3-10: Spectrometer Image of AgGaS<sub>2</sub> Output

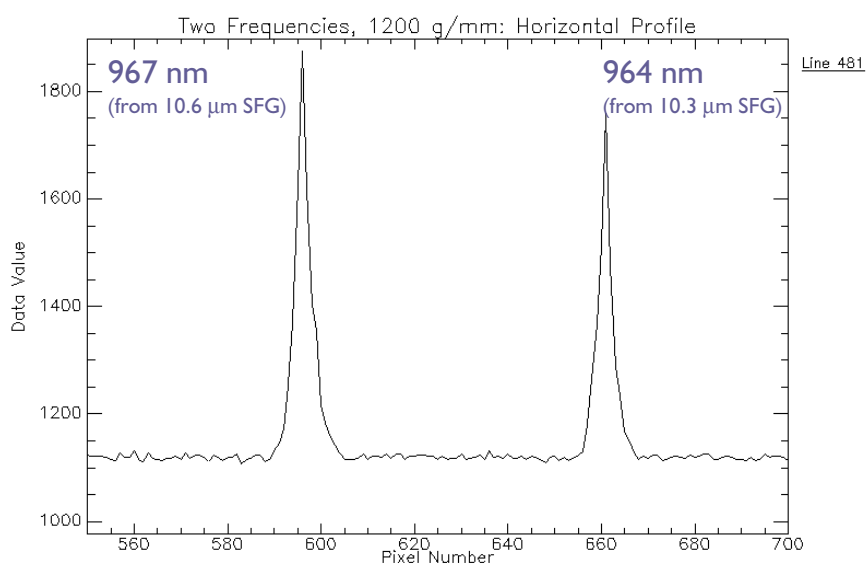


Figure 3-11: One Line of Spectrometer Data, AgGaS<sub>2</sub> Output

#### 3.2.4.4 *Detection of Modulation*

The first phase was designed with sufficient power to accommodate one upconversion, and the modulation was to be analyzed spectrally. No spectral effects of the 1 THz modulation were detected in the output of the AgGaS<sub>2</sub> crystal.

### **3.3 Phase 2: SFG Using 100 ps CO<sub>2</sub> Pulses**

A second phase of the experiment was constructed in order to provide sufficient power to try other methods of detecting the 1 THz modulation (Sections 4, 5). Two experimental setups were used, since the first did not provide scanning of the phase matching angle. (Section 3.3.1.1) The scanning of this angle is necessary to measure the acceptance angle (Figures 2-7, 3-1).

#### **3.3.1 Experimental Setup**

The longer, 100 ps CO<sub>2</sub> pulse was used for this experiment, instead of the short pulse train (Figure 1-3). The need for the fiber optic delay line was eliminated by not using the second stage of amplification of the CO<sub>2</sub> pulses, and, thus, the limits on the 1  $\mu$ m power imposed by the damage threshold of the fiber were exchanged for the higher damage threshold of AgGaS<sub>2</sub>. A bandpass filter centered at 970 nm with a FWHM of 10 nm was used to prevent any residual 1 or 10  $\mu$ m power transmitted by AgGaS<sub>2</sub> from reaching the KDP crystal.

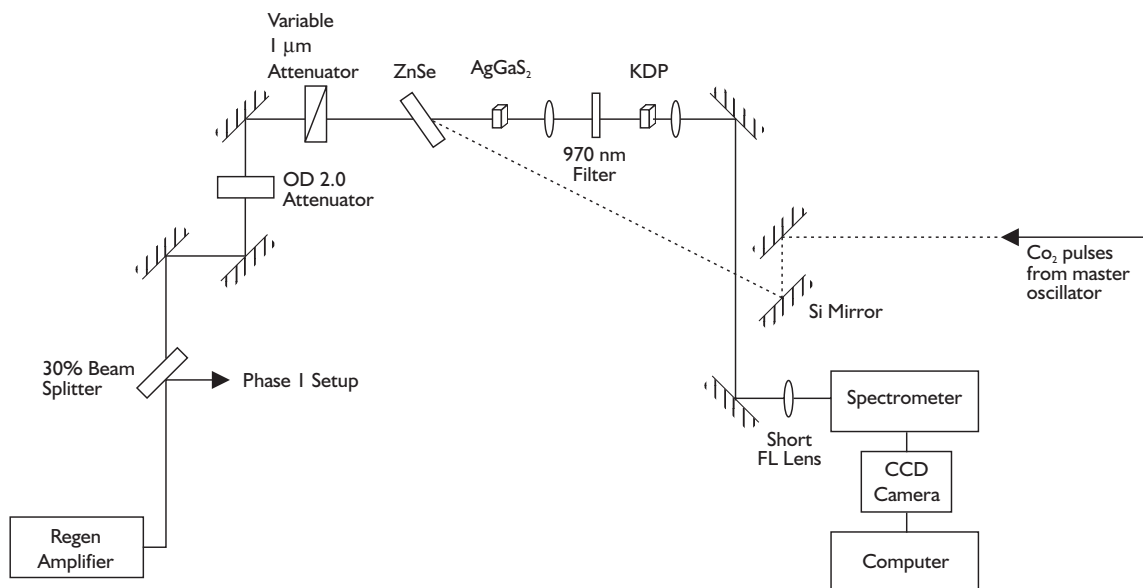


Figure 3-12: Phase 2: First Experimental Setup

### 3.3.1.1 Crystal Orientation

When the AgGaS<sub>2</sub> crystal was received by the lab, no documentation was present to indicate the orientation of the crystal's optical axis. During the first and second phases of the project, the crystal's orientation was determined by the efficiency of SFG - i.e., the crystal was rotated until the face yielding the highest efficiency was found. Since the incident polarization was ordinary in each setup, each experienced the same Type I ooe SFG interaction with the same output wavelengths and the same efficiency; however, the position of the stage in the first setup did not allow the phase matching angle to be scanned. Once the rotational stage was correctly positioned, the acceptance angle was measured. (Figure 3-16)

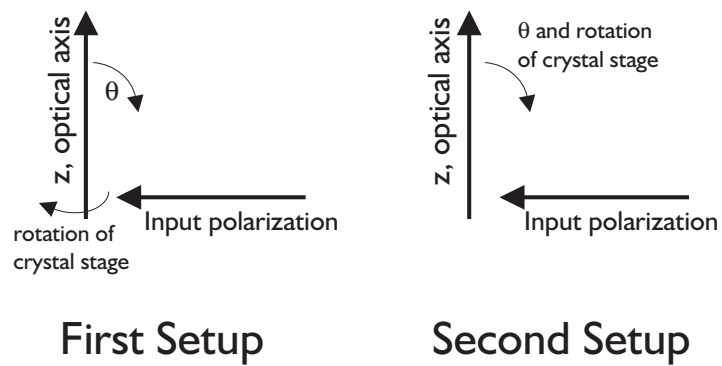


Figure 3-13: Crystal Orientation for Phase Matching Angle Scan

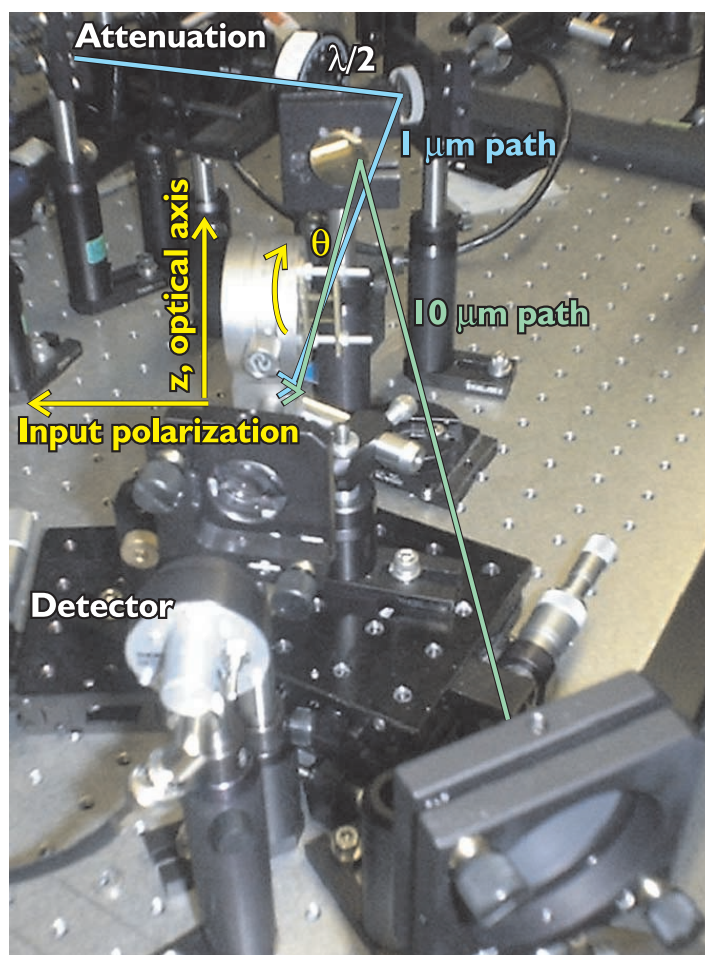


Figure 3-14: Photo of Second Setup for Phase 2

### 3.3.2 Theoretical Efficiency and Output Power

The purpose of this setup was to provide a higher output power - which differs from the efficiency of the nonlinear interaction. The power of the output wave is controlled by the amount of the medium used (length and area) and by the intensity of the incident waves; thus, an interaction with a lower efficiency may still yield a high output power if the interaction area is large or the crystal is long and the incident waves have high powers.

The primary difference between this setup and the previous one is that this setup used unfocused beams to interact within the crystal; whereas, the first setup used focused beams. To develop a permanent system, one would have to optimize the output power of the crystal by testing both the focused and unfocused geometries.

Measurements indicate that Phase 1 delivered 0.04 MW (4  $\mu$ J) of 1  $\mu$ m light to the crystal, whereas Phase 2 delivered 100 MW (10 mJ). The efficiency of the interaction in Phase 2 was calculated as 0.0091% for 10.27  $\mu$ m and for 10.59  $\mu$ m. Regardless of having 15 times less efficiency, the output power of the crystal for Phase 2 was theoretically predicted to be 100 times greater than that for Phase 1. This would provide sufficient output power to up-convert the 964 and 967 nm light in KDP. (Section 4)

### 3.3.3 Experimental Data

Two sets of data were taken - one to verify that the output intensity varied linearly with the input energy (using the first setup) and the other to examine  $\text{sinc}^2$  function in the intensity profiles of the 964 and 967 nm light (using the second setup). The intensity in the 967 nm wave varied linearly with the input energy.

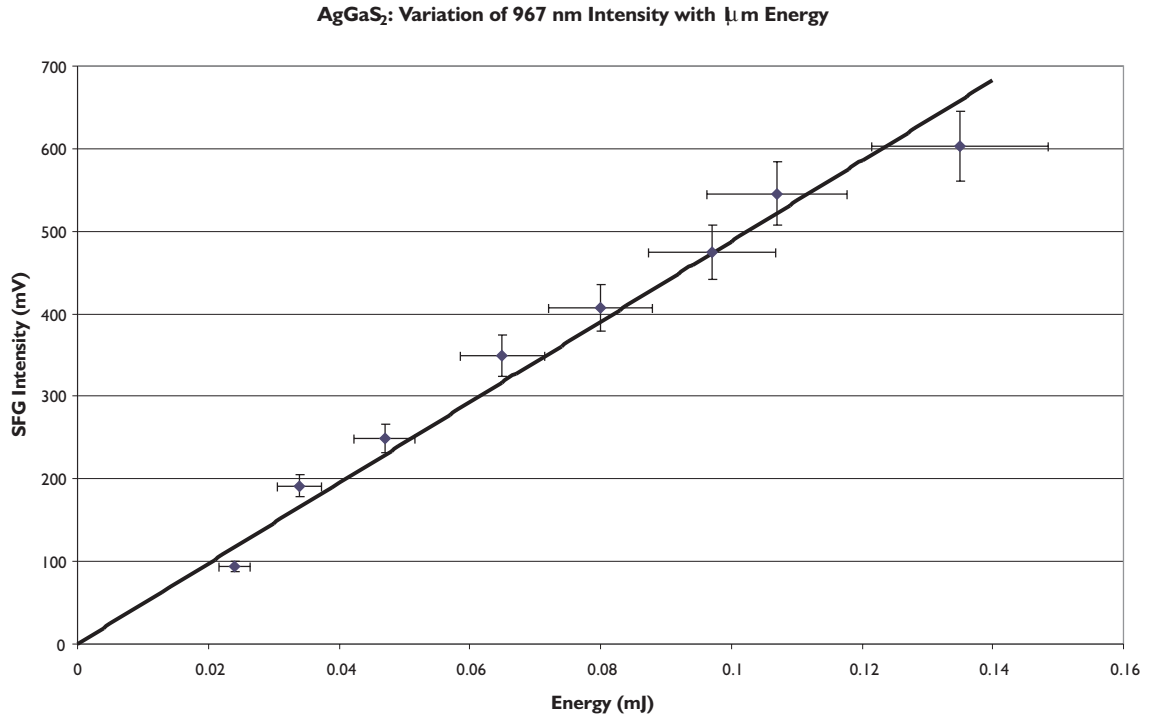


Figure 3-15: AgGaS<sub>2</sub> Output Intensity Variation with 1  $\mu\text{m}$  Input Energy

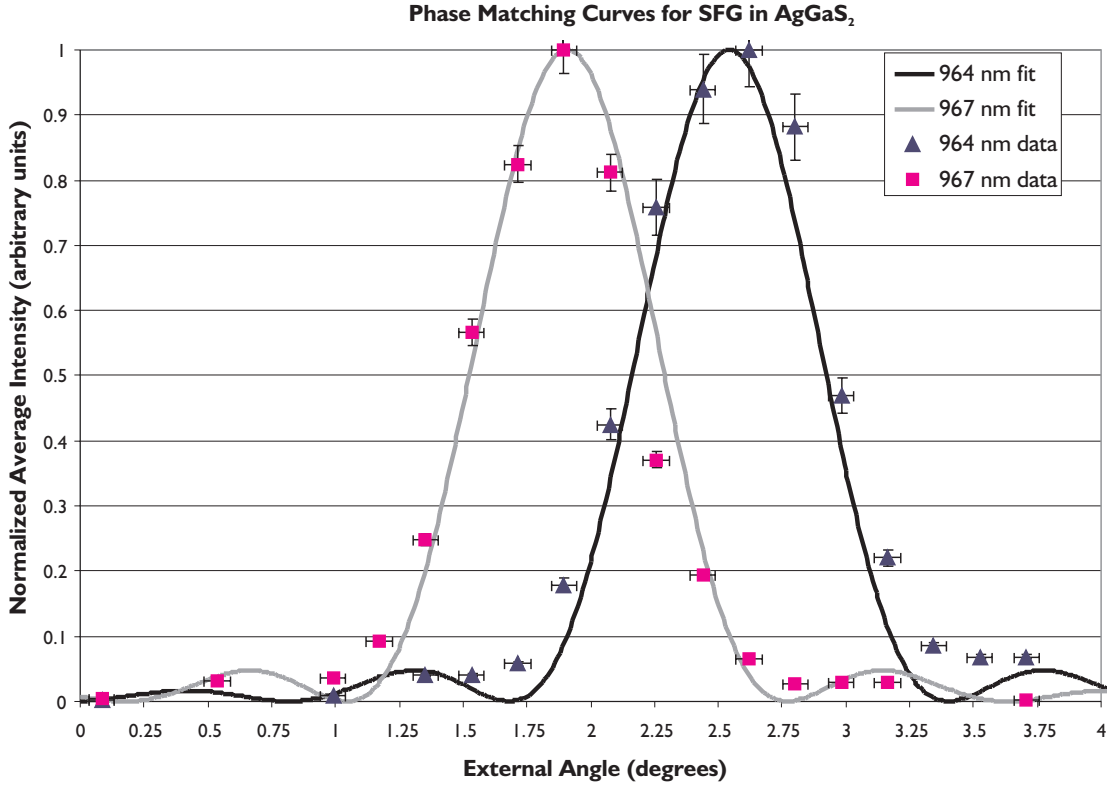


Figure 3-16: Angular Dependence of SFG Output in AgGaS<sub>2</sub>

### 3.3.3.1 Non-Collinear Phase Matching in AgGaS<sub>2</sub>

SFG was also achieved in the AgGaS<sub>2</sub> crystal using non-collinear phase matching. This layout eliminated the need for the ZnSe beam combiner, which made the crystal's surface damage threshold the limiting factor in the system. Previously the power level in the system was determined by first the damage threshold of the optical fiber and second by that of the ZnSe.

The non-collinear phase matching setup, Figure 3-17, was used to measure the efficiency of SFG and the SFG output data for Figure 3-16. The efficiency of the interaction was also measured, Section 3.3.3.1.1.

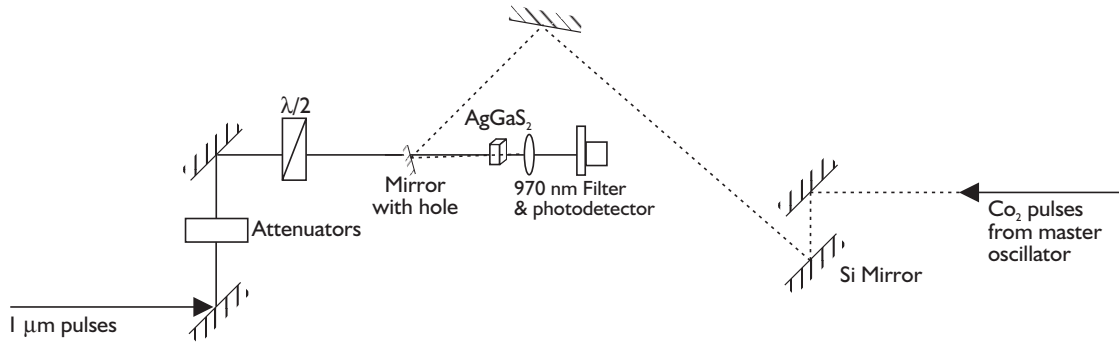


Figure 3-17: Non-Collinear Phase Matching, Experimental Setup

#### 3.3.3.1.1 Efficiency: Non-Collinear Phase Matching

The efficiency of this setup was measured using a silicon photodiode, as follows:

Background = 20 mV

1  $\mu\text{m}$  pulses: 159 mV with  $10^6$  attenuation

SFG output of  $(10.59 \mu\text{m} + 1.04 \mu\text{m} = 967 \text{ nm})$ : 62 mV with  $10^4$  attenuation

This efficiency is roughly 0.3%, neglecting the CO<sub>2</sub> input, and is consistent with the efficiencies measured in the first phase ( $\sim 0.12\%$ ) and the theoretically predicted efficiency ( $\sim 0.2\%$ ). This demonstrated that the noncollinear setup produces equivalent results as that which include the ZnSe beam combiner.

### **3.4 Summary**

The results from this study included the characterization of SFG in  $\text{AgGaS}_2$ , as well as much experience working with the crystal. Detecting the 1 THz modulation proved to be more difficult than originally expected and provided the motivation for the autocorrelator (Section 5.3). Conclusions from this work included:

In  $\text{AgGaS}_2$ , the phase matching curves for generating 967 and 964 nm light by SFG are sufficiently overlapped that the interactions can be simultaneously phase matched.

The proper orientation of the optical axis of an unknown crystal and, subsequently, the angles through which all rotational stage scan, should not be determined by only using the efficiency of a nonlinear interaction, but by an angle dependent measurement, such as scanning the SFG output.

SFG in the short crystal may be achieved by either collinear or noncollinear phase matching, with similar output powers. Using noncollinear phase matching avoids the use of a beam combiner with a damage threshold lower than that of the crystal, allowing for higher input powers.

## 4 UP-CONVERSION IN KDP

In order for the 1 THz modulation to exist, the three waves incident on the AgGaS<sub>2</sub> crystal must be simultaneous in both time and space. To confirm this, the light resulting from SFG in the AgGaS<sub>2</sub> was up-converted using a KDP crystal. If the waves resulting from SFG in AgGaS<sub>2</sub> are spatially and temporally simultaneous, then the up-conversion in KDP results in three waves<sup>43</sup>: 483.4 nm (SHG of 967 nm), 482.7 nm (SFG of 967 nm and 964 nm), and 482.0 nm (SHG of 964 nm).

### 4.1 Theoretical Analysis

The KDP crystal is transparent to wavelengths between 0.178 and 1.45  $\mu\text{m}$ ,<sup>2</sup> which makes it suitable for the second up-conversion. In addition, the phase matching angles for the interactions of interest are sufficiently similar and within the acceptance angles to make phase matching of more than one interaction feasible. (e.g., SFG of 1  $\mu\text{m}$  and 967 nm as well as SFG of 1  $\mu\text{m}$  and 964 nm). The group velocity mismatch (GVM) between the 964 nm pulses and the SHG output, 482 nm, is 0.8 ps/cm - small enough to maintain the 1 THz modulation over the length of the crystal. (Refer to Section 3.1 for more details.)

1 cm crystal 8 mm spot size	Phase Matching Angle (deg., int)	Acceptance Angle (deg., int)	% Efficiency
SHG ,1 $\mu\text{m}$	41.208	0.0631	5.6E-07
SHG, 967 nm	41.411	0.0564	1.9E-09
SHG, 964 nm	41.432	0.0562	1.9E-09
SFG: 964 & 967 nm	41.421	0.0563	3.9E-09
SFG: 1 $\mu\text{m}$ & 967 nm	41.186	0.0596	1.2E-06
SFG: 1 $\mu\text{m}$ & 964 nm	41.120	0.0595	1.2E-06

Table 4-1: Theoretical Parameters for SHG, SFG in KDP

## 4.2 Experimental Data

The diagram for the setup is provided in Figure 3-11. The three output waves were detected using the spectrometer and CCD camera, using a 1200 grooves/mm grating and a 64  $\mu\text{m}$  slit. The difference in output power was theoretically predicted, with the efficiency of SFG between 964 and 967 nm four times that for SHG of either. This difference was verified experimentally, where the output power of SFG was 3 to 4 times that of the SHG. From these results, it was inferred that the second stage of up-conversion (Figure 1-1) would use SFG, instead of SHG - most likely SFG of the 1  $\mu\text{m}$  pulses and the output of the AgGaS<sub>2</sub> crystal.

This particular setup used a long CO<sub>2</sub> pulse which was gated by the 1  $\mu$ m pulse; however, in the future, the up-conversion of the 964 and 967 nm outputs in KDP could be used to demonstrate that the pulses incident upon the AgGaS<sub>2</sub> crystal and spatially and temporally simultaneous.

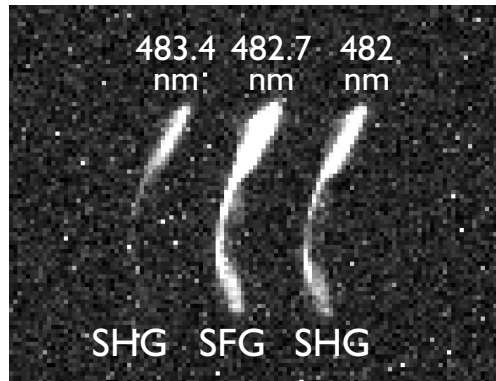


Figure 4-1: Up-Conversion in KDP, Image

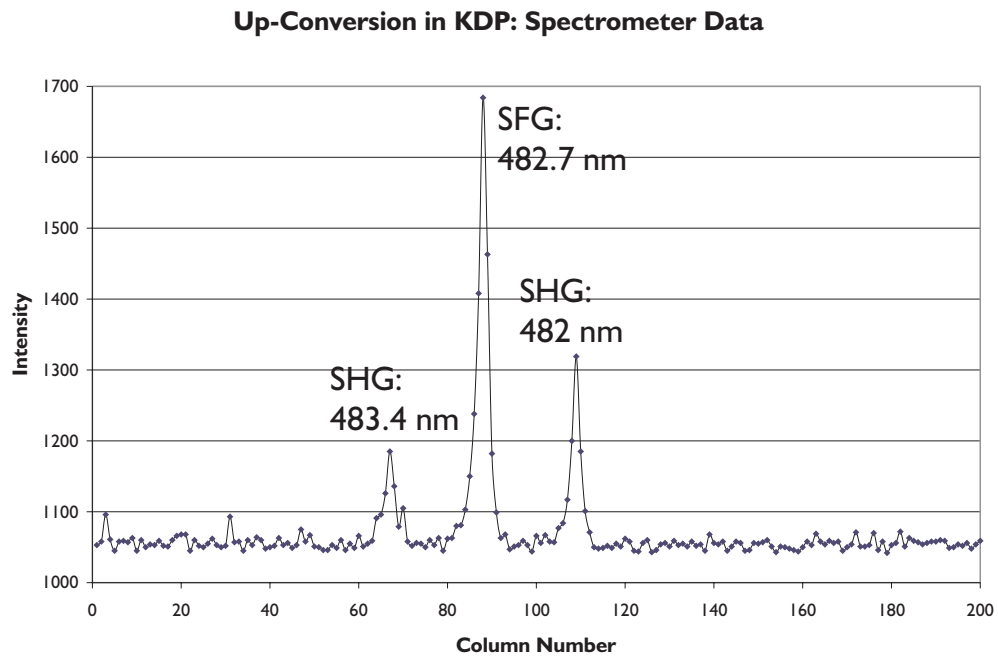


Figure 4-2: Upconversion in KDP, Data

## 5 DETECTION OF MODULATION: AUTOCORRELATION

The purpose of an autocorrelator is to spatially map the temporal structure of a laser pulse. This is accomplished by splitting the pulse into two paths, delaying one of them, and recombining the paths through noncollinear phase matching in a nonlinear crystal, such as KDP. The first autocorrelator used in the experiment was built by Positive Light (Section 5.2). When this autocorrelator proved to not work for dual frequency detections, a second autocorrelator was designed and built. (Section 5.3) This will be used in future work on this project, in either a single-shot or a multi-shot mode. (Section 5.4)

### 5.1 Background

An autocorrelator is used to examine the temporal structure of the laser pulse, using the intensity autocorrelation function, below.<sup>44</sup>

$$\text{Autocorrelation} = A(\tau) = \int_{-\infty}^{\infty} I(t)I(t + \tau)dt \quad (5.1)$$

Two types of autocorrelators have been considered for this project - single shot and multi-shot. Each uses a nonlinear crystal to provide the autocorrelation signal, by SHG of the pulse with a shifted version of itself. The difference between the multi-shot and single-shot configurations is the way in which the autocorrelation signal is measured.

In the multi-shot configuration, the autocorrelation signal is measured by scanning the shifted pulse through the original pulse, using an interferometer. The delay,  $\Delta\tau$ , is provided by the scanning mirror, such that  $\Delta\tau = \frac{\sqrt{2}d}{c}$ , where d is the diameter

of the mirror and  $c$  is the speed of light. This setup requires that the pulse repetition rate be much greater than the scan rate.<sup>36</sup> The resulting autocorrelation trace can be measured in many ways, such as by a CCD<sup>45</sup> or photomultiplier<sup>46</sup>.

In a single-shot autocorrelator, the autocorrelation function is measured once per shot, using the spatial pattern resulting from noncollinear SHG of the pulse and the shifted version of itself. Physically, the time delay between the two pulses is different at every point in the crystal. When the light resulting from noncollinear SHG at each point is measured, the effect is to provide “integration” of the incident pulses similar to that which is obtained by scanning in multi-shot systems.<sup>36,47</sup>

When the result of noncollinear SHG is measured, the width of the pulse,  $\Delta w$ , corresponds to a specific amount of time,  $\Delta\tau$ . These quantities are related by the crystal’s index of refraction at the incident wavelength,  $n$ , the speed of light,  $c$ , and the angle between the two incident pulses,  $2\theta$ , as:<sup>48</sup>

$$\Delta w = \frac{c\Delta\tau}{n \sin \theta} \quad (5.2)$$

When designing a single shot autocorrelator, one must keep the detector close to the crystal to avoid destructive interference<sup>40</sup>, and use a beam diameter that is at least 2/3 larger than the length of the pulse within the crystal,  $c\tau/n$ .<sup>40,49</sup>

## 5.2 Commercial Autocorrelator

The first single-shot autocorrelator used was made by Positive Light. This autocorrelator has two modes, differing by one component in the path used to delay one part of the pulse. One setup uses a mirror to measure fempto-second pulses (Model SSA-F) and the other uses a grating to measure picosecond pulses (Model SSA-P).<sup>50</sup> Since the modulation in this project should vary on the order of 1 ps, the SSA-P model was used. The autocorrelator was used in place of the spectrometer, as in the figure below.

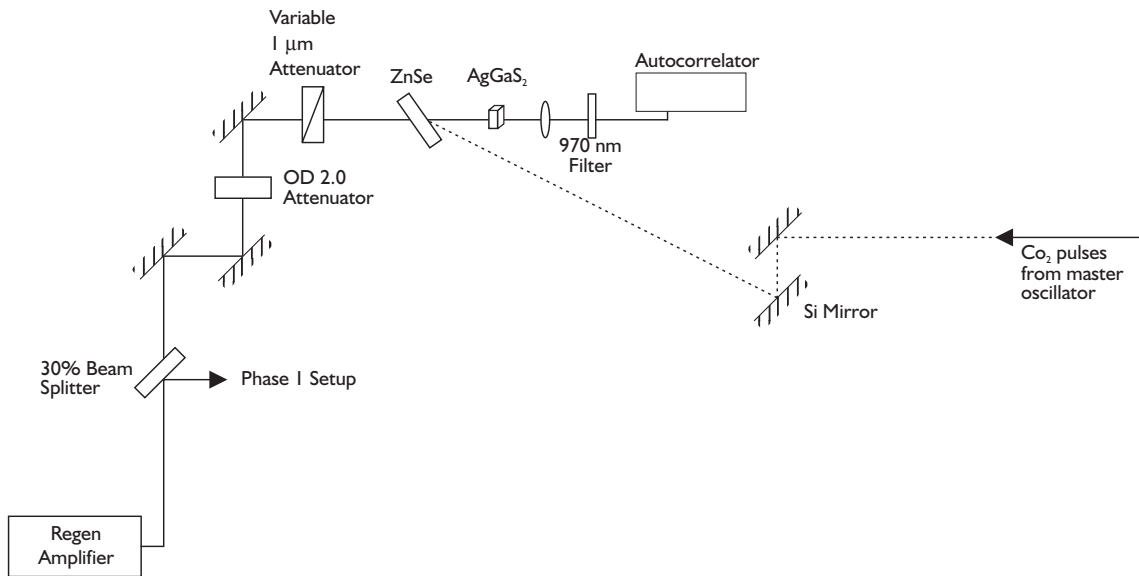


Figure 5-1: Experimental Setup for Autocorrelation

The operation of the autocorrelator was tested using the Nd:YAG pulse (without the AgGaS<sub>2</sub> crystal). The oscilloscope traces below show the two collinear SHG pulses (1.064  $\mu\text{m}$   $\rightarrow$  532 nm), and the noncollinear SHG pulse. These were obtained by rotating the KDP crystal in the SSA-P autocorrelator - adjusting the

phase matching angle for first one collinear SHG pulse, next for the noncollinear SHG pulse, then the other collinear SHG pulse. The structure in the traces is due to the beam profile of the Nd:YAG laser. 1 M $\Omega$  termination on the oscilloscope was required to read data from the CCD. The 100 ps Nd:YAG pulse was too long to be used for characterizing the autocorrelator, but this procedure demonstrated how one would verify the device's operation in the future.

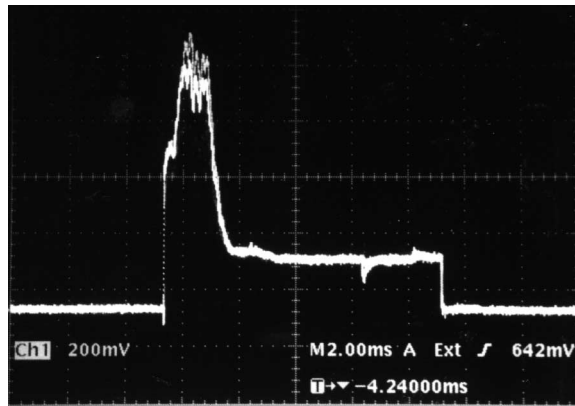


Figure 5-2: Collinear SHG in SSA with 1  $\mu$ m Pulse, Path 1

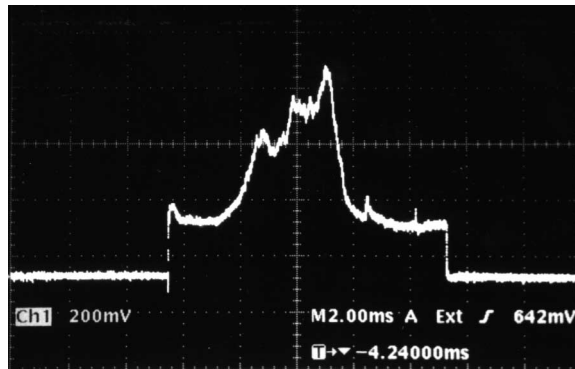


Figure 5-3: Noncollinear SHG with two 1  $\mu$ m Pulses

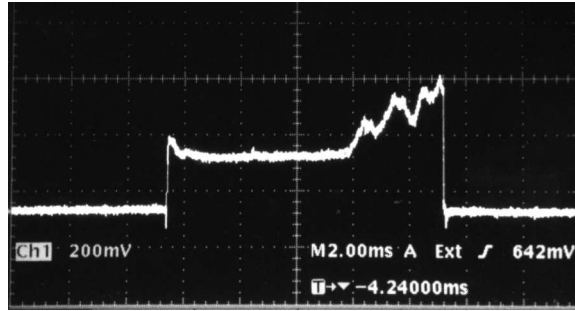


Figure 5-4: Collinear SHG in SSA with 1  $\mu\text{m}$  Pulse, Path 2

Two problems arose when this autocorrelator was used to detect the 1 THz modulation:

- 1) The result of up-converting the output of the  $\text{AgGaS}_2$  crystal in KDP was sufficiently strong to be detected using a CCD, but not a photodiode.
- 2) In a different experiment performed by our lab group, it was discovered that the grating spatially separated the incident wavelengths. Since these wavelengths must be spatially and temporally overlapped to maintain the 1 THz modulation, the SSA-P model would not be suitable for detecting the modulation in the output of the  $\text{AgGaS}_2$  crystal.

### 5.3 Custom Autocorrelator Design

A custom autocorrelator was redesigned, from an older setup, and tested; however, due to time constraints, the output of the  $\text{AgGaS}_2$  crystal was not measured using this autocorrelator.

### 5.3.1 Experimental Setup

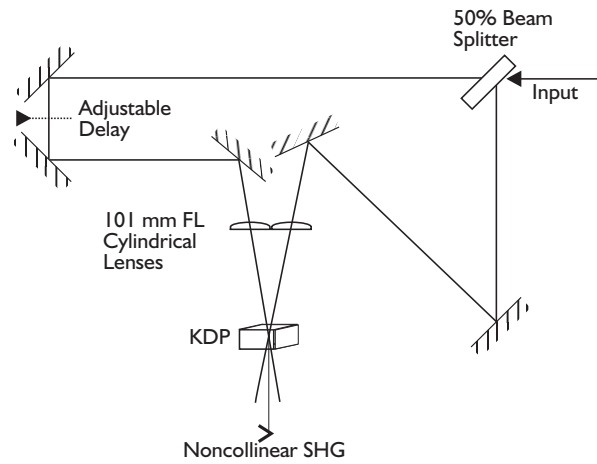


Figure 5-5: Block Diagram of Custom Autocorrelator

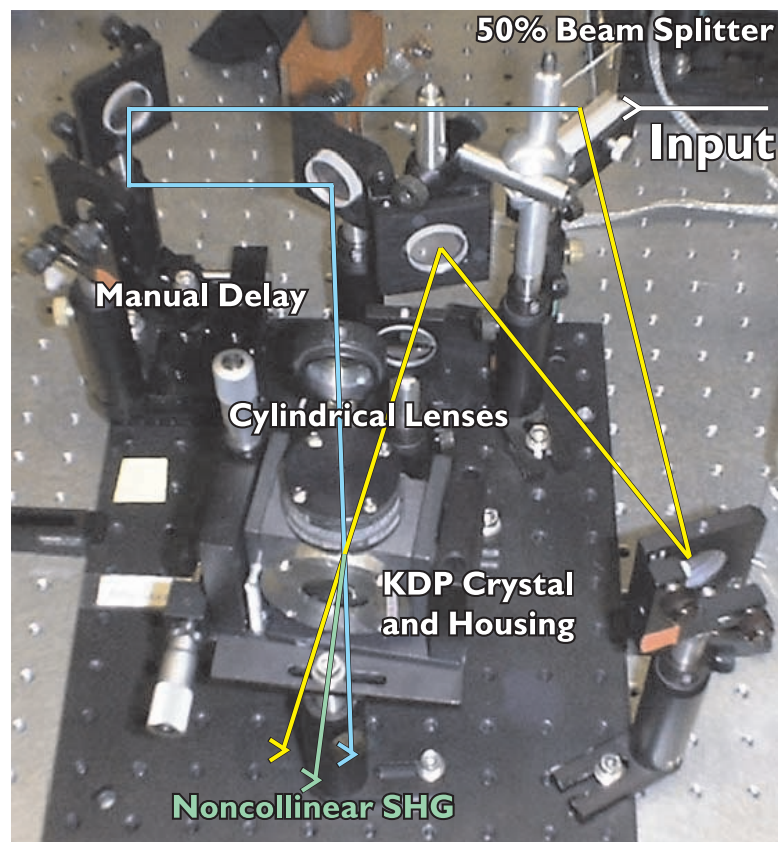


Figure 5-6: Photo of Custom Autocorrelator

### 5.3.2 Experimental Design

The custom autocorrelator was designed using non-dispersive elements and a 2.5 cm KDP crystal. Two cylindrical lenses with 10 cm focal lengths were used to focus the pulses to a line, in order to increase their intensity. A line was used instead of a point to preserve the width of the beams (Section 5.1). The 2.5 cm KDP crystal was used because it had a sufficiently large aperture to accommodate the widths of the incident pulses.

To calculate the width of the autocorrelation window, the intersection angle between the pulses was measured -  $22.6^\circ$ . ( $\theta = 11.3^\circ$ , external to the crystal) This corresponds to an internal angle of  $7.6^\circ$  (by dividing the external angle by  $n_o = 1.49$  for  $1\text{ }\mu\text{m}$  in KDP). Using this angle, a beam width of 8 mm corresponds to an autocorrelation window of 5.25 ps. For an 8 mm-wide beam, this corresponds to a resolution of approximately 0.6 ps/mm at the CCD. This should be sufficient to detect the 1 ps beatwave modulation.

### 5.3.3 Future Work

The custom autocorrelator has been built and tested. For detection of the 1 THz pulses, it can be used as either a “single-shot” or “multi-shot” autocorrelator. The single-shot autocorrelation scheme is preferable - since the modulation is detected using one laser pulse, the measurement errors are less. If there is insufficient power to detect the output on a CCD, a “multi-shot” configuration can be created by replacing the CCD with a photodiode. The laser pulses incident on the KDP crystal would then be scanned through each other manually, using the micrometer on the delay line. The data would be the average intensity of noncollinear SHG at each point, as measured by the photodiode.

## 6 CONCLUSION

This project accomplished some of its original goals by realizing two stages of up-conversion - in  $\text{AgGaS}_2$  and KDP - and established an experimental configuration for up-converting the THz modulation in nonlinear crystals. A clear path has been left for future work - including an operating autocorrelator for use with a 6 ps Nd:YAG pulse. (Section 5)

## 7 REFERENCES

- 1 Clayton, C., et al. "Second Generation Beatwave Experiments at UCLA". Nuclear Instruments & Methods in Physics Research, Section A. Vol 410, No 3. pp 378-387. 1998.
- 2 Lal, A. et al. "Measurement of the Beatwave Dynamics in Time and Space". Proceedings of the 1995 Particle Accelerator Conference. Vol 2, No 5. pp 767-769.
- 3 Hankla, A.K. et al. "Tunable Short-Pulse Beat-wave Laser Source Operating at 1 mm". Optics Letters. Vol 22, No 22. pp 1713-1715. November, 1997.
- 4 Tochitsky, S. Y., et al. "Generation of 160-ps Terawatt-Power CO<sub>2</sub> Laser Pulses". Optics Letters. Vol 24, No 23. pp 1717-1719. 1999.
- 5 Dmitriev, V.G., G.G. Gurzadyan, and D.N. Nikogosyan, eds. Handbook of Nonlinear Optical Crystals. 3rd ed. Berlin: Springer-Verlag, 1999.
- 6 Shen Y.R. The Principles of Nonlinear Optics. New York: John Wiley & Sons, Inc., 1984.
- 7 Sauter, E.G., Nonlinear Optics. New York: John Wiley & Sons, Inc., 1996.
- 8 Lauberau, Alfred. "Optical Nonlinearities with Ultrashort Pulses". Topics in Applied Physics: Ultrashort Laser Pulses. Vol 60. Ed. W. Kaiser. New York: Springer-Verlag, 1993.

- 9 Glenn, W.H. "Second-Harmonic Generation by Picosecond Optical Pulses". IEEE Journal of Quantum Electronics. Vol QE-5, No 6. pp 284-290. 1969.
- 10 Bhar, G.C., S. Das, and P.K. Datta. "Tangentially phase-matched infrared detection in AgGaS<sub>2</sub>". Journal of Physics D: Applied Physics. Vol 27. pp. 228-230. 1994.
- 11 Voronin, E.S. et al. "Conversion of Infrared Radiation in an AgGaS<sub>2</sub> Crystal". Soviet Journal of Quantum Electronics. Vol 5, No 5. pp 597-598. 1975.
- 12 Bhar, G.C., et al. "Synchronous and Noncollinear Infrared Upconversion in AgGaS<sub>2</sub>". Applied Physics Letters. Vol 54, No 16. pp 1489-1491. 1989.
- 13 Boyd, G.D., H. Kasper, and J.H. McFee. "Linear and Nonlinear Optical Properties of AgGaS<sub>2</sub>, CuGaS<sub>2</sub>, and CuInS<sub>2</sub>, and Theory of the Wedge Technique for the Measurement of Nonlinear Coefficients". IEEE Journal of Quantum Electronics. Vol QE-7, No 12. pp. 563-573. December, 1971.
- 14 McEwan, K.J. "High-power Synchronously Pumped AgGaS<sub>2</sub> Optical Parametric Oscillator". Optics Letters. Vol 23, No 9. pp 667-669. May, 1998.
- 15 Roberts, D.A. "Simplified Characterization of Uniaxial and Biaxial Nonlinear Optical Crystals: A Plea for Standardization of Nomenclature and Conventions". IEEE Journal of Quantum Electronics. Vol 28, No 10. pp 2057-2074. October, 1992.

- 16 Cleveland Crystals, material properties table,  
<http://www.clevelandcrystals.com/AGSSE.shtml#table>
- 17 Zondy, J.J. and D. Touahri. "Updated Thermo-Optic Coefficients of  $\text{AgGaS}_2$  from Temperature-Tuned Noncritical  $3\omega - \omega \rightarrow 2\omega$  Infrared Parametric Amplification". Journal of the Optical Society of America B. Vol 14, No 6. pp 1331-1338. June, 1997.
- 18 Nikogosyan, D.N. "Nonlinear Optical Crystals (Review and Summary Data)". Soviet Journal of Quantum Electronics. Vol 7, No 1. pp 1-12. January, 1977.
- 19 Fan, Y.X., et al. " $\text{AgGaS}_2$  Infrared Parametric Oscillator". Applied Physics Letters. Vol 45, No 4. pp 313-315. August, 1984.
- 20 Bhar, G.C. et al. "Phasematching of Infrared Nonlinear Laser Devices Using  $\text{AgGaS}_2$ ". IEEE Journal of Quantum Electronics. Vol 24, No 8. pp 1492-1494. August, 1988.
- 21 Cheevers, Elizabeth. Corning Optical Fiber Information Center, Private Communication. February, 2000.
- 22 Milam, D. "1064-nm Laser Damage Thresholds of Polished Glass Surfaces as a Function of Pulse Duration and Surface Roughness". Symposium on Optical Materials for High Power Lasers. Boulder, Colorado. September 12-14, 1978.

- 23 Milam, D. "Laser Induced Damage at 1064 nm, 125 psec". Applied Optics, Vol 16 No 5. pp 1204-1208. May, 1977.
- 24 Jahn, L.A. Gomez, J.J. Kasinski, and R.J. Dwayne Miller. "High-Energy Handling Capabilities of Optical Fibers: Application to Pulse Compression and Direct Generation of Megawatt Picosecond Pulses". Applied Physics A. Vol 43. pp 41-46. 1987.
- 25 General Fiber Optics, Inc. Catalog, 1985.
- 26 Rainer, F. E.A. Hildum, and D. Milam. "Database of Average-Power Damage Thresholds at 1064 nm". The Boulder Damage Symposium. October 26-28, 1987.
- 27 Allison, S.W., et al. "Pulsed Laser Damage to Optical Fibers". Applied Optics. Vol 24, No 19. pp 3140-3145. October, 1985.
- 28 Art Photonics, <http://www.jtingram.com/art/hipo.html>
- 29 Crow, John D. "Power Handling Capability of Glass Fiber Lightguides". Applied Optics. Vol 13, No 3. pp 467-468. 1974.
- 30 Siegman, Anthony E. Lasers. California: University Science Books. 1986.
- 31 Kim, K.S. et al. "Measurement of the Nonlinear Index of Silica-Core and Dispersion-Shifted Fibers". Optics Letters, Vol 19, No 4. pp 257-260. 1994.

- 32 Boskovic, A. et al. "Direct Continuous-Wave Measurement of  $n_2$  in Various Types of Telecommunications Fiber at 1.55  $\mu\text{m}$ ". Optics Letters, Vol 21, No 24. pp 1966-1967. 1996.
- 33 Thorlabs Company Catalog, [www.thorlabs.com](http://www.thorlabs.com)
- 34 Kawano, K., H. Miyazawa, and O. Mitomi. "New Calculations for Coupling Laser Diode to Multimode Fiber". Journal of Lightwave Technology. Vol LT-4, No 3. pp. 368-374. March, 1985.
- 35 Continuum technical support. Model number RGA69-10. March, 2000.
- 36 II-VI, Inc. <http://www.iivi.com/pages/res-determining.html>
- 37 Yeh, C. Handbook of Fiber Optics: Theory and Applications. New York: Academic Press, Inc. 1990.
- 38 Weik, M.H. Fiber Optics Standard Dictionary, 3rd ed. New York: Chpman & Hall. 1997.
- 39 Wave Optics, Inc.  
[http://www.waveoptics.com/Accessories.html#Accessory\\_Fiber\\_Anchor](http://www.waveoptics.com/Accessories.html#Accessory_Fiber_Anchor)
- 40 Herriot, D.R. and H.J. Schulte. "Folded Optical Delay Lines". Applied Optics. Vol 4, No 8. pp 883-889. August, 1965.

- 41 McManus, J.B., P.L. Kebabian, and M.S. Zahniser. "Astigmatic Mirror Multipass Absorption Cells for Long-Path-Length Spectroscopy". *Applied Optics*. Vol 34, No 18. pp 3336-3348. June, 1995.
- 42 Reeder, Robin. "Slab Amplifier Design". Hughes Aircraft, 1992.
- 43 Bass, M. et al. "Optical Mixing". *Physical Review Letters*. Vol 8, No 1. p 18. 1962.
- 44 Collier, J. et al. "Uniaxial Single Shot Autocorrelator". *REview of Scientific Instruments*. Vol 70, No 3. pp 1599-1602. 1999.
- 45 Yasa, Z.A. and N.M. Amer. "A Rapid-Scanning Autocorrelator Scheme for Continuous Monitoring of Picosecond Laser Pulses". *Optics Communications*. Vol 36, No 2. pp 406-408. 1981.
- 46 Watanabe, A. et al. "A Rapid-Scanning Interferometric Autocorrelator for Monitoring Femptosecond Pulses". *Optics Communications*. Vol 69, No 5-6. pp 405-408. 1989.
- 47 Jansky, J., G. Corradi, and R.N. Gyuzalian. "On a Possibility of Analyzing the Temporal Characteristics of Short Light Pulses". *Optics Communications*. Vol 23, No 3. pp 293-298. 1977.
- 48 Rempel, C. and W. Rudolph. "Single Shot Autocorrelator for Femptosecond Pulses". *Experimentelle Technik der Physik*. Vol 37. pp 381-385. 1989.

- 49 Kolmeder, C., W. Zinth, and W. Kaiser. "Second Harmonic Beam Analysis: A Sensitive Technique to Determine the Duration of Single Ultrashort Pulses". Optics Communications. Vol 30, No 3. pp 473-457. 1979.
- 50 User's Manual for the Positive Light Autocorrelators, Models SSA-P and SSA-F. [www.poslight.com](http://www.poslight.com)